Contrib Mineral Petrol (2014) 168:1078
DOI 10.1007/s00410-014-1078-3

ORIGINAL PAPER

Quaternary bimodal volcanism in the Niğde Volcanic Complex (Cappadocia, central Anatolia, Turkey): age, petrogenesis and geodynamic implications

Faruk Aydin · Axel K. Schmitt · Wolfgang Siebel · Mustafa Sönmez · Yalçın Ersoy · Abdurrahman Lermi · Kadir Dirik · Robert Duncan

Received: 12 June 2014 / Accepted: 20 October 2014 / Published online: 4 November 2014

Abstract The late Neogene to Quaternary Cappadocian Volcanic Province (CVP) in central Anatolia is one of the most impressive volcanic fields of Turkey because of its extent and spectacular erosionally sculptured landscape. The late Neogene evolution of the CVP started with the eruption of extensive andesitic-dacitic lavas and ignimbrites with minor basaltic lavas. This stage was followed by Quaternary bimodal volcanism. Here, we present geochemical, isotopic (Sr–Nd–Pb and $\delta^{18}O$ isotopes) and geochronological (U–Pb zircon and Ar–Ar amphibole and whole-rock ages) data for bimodal volcanic rocks of the Niğde Volcanic Complex (NVC) in the western part of the CVP to determine mantle melting dynamics and magmatic processes within the overlying continental crust during the Quaternary. Geochronological data suggest that the bimodal volcanic activity in the study area occurred between ca. 1.1 and ca. 0.2 Ma (Pleistocene) and comprises (1) mafic lavas consisting of basalts, trachybasalts, basaltic andesites and scoria lapilli fallout deposits with mainly basaltic composition, (2) felsic lavas consisting of mostly rhyolites and pumice lapilli fall-out and surge deposits with dacitic to rhyolitic composition. The most mafic sample is basalt from a monogenetic cone, which is characterized by $^{87}Sr/^{86}Sr = 0.7038$, $^{143}Nd/^{144}Nd = 0.5128$, $^{206}Pb/^{204}Pb = 18.80$, $^{207}Pb/^{204}Pb = 15.60$ and $^{208}Pb/^{204}Pb = 38.68$, suggesting a moderately depleted signature of the mantle source. Felsic volcanic rocks define a narrow range of $^{143}Nd/^{144}Nd$ isotope ratios (0.5126–0.5128) and are homogeneous in Pb isotope composition ($^{206}Pb/^{204}Pb = 18.84$–$18.87$, $^{207}Pb/^{204}Pb = 15.64$–$15.67$ and $^{208}Pb/^{204}Pb = 38.93$–$38.99$). $^{87}Sr/^{86}Sr$ isotopic compositions of mafic (0.7038–0.7053) and felsic (0.7040–0.7052) samples are similar, reflecting a common mantle source. The felsic rocks have relatively low

Communicated by J. Hoefs.

Electronic supplementary material The online version of this article (doi:10.1007/s00410-014-1078-3) contains supplementary material, which is available to authorized users.

F. Aydin (✉)
Department of Geological Engineering, Karadeniz Technical University, 61080 Trabzon, Turkey
e-mail: faydin61@gmail.com; faydin@ktu.edu.tr

A. K. Schmitt
Department of Earth, Planetary, and Space Sciences, University of California, Los Angeles, 595 Charles Young Drive East, Los Angeles, CA 90095-1567, USA

W. Siebel
Department of Geosciences, Universität Tübingen, Wilhelmstr. 56, 72074 Tübingen, Germany

M. Sönmez · A. Lermi
Department of Geological Engineering, Niğde University, 51200 Niğde, Turkey

Y. Ersoy
Department of Geological Engineering, Dokuz Eylül University, 35160 Izmir, Turkey

K. Dirik
Department of Geological Engineering, Hacettepe University, 06800 Ankara, Turkey

R. Duncan
College of Oceanic and Atmospheric Sciences, Oregon State University, Corvallis, OR 97331-5503, USA

zircon $\delta^{18}O$ values (5.6 ± 0.6 ‰) overlapping mantle values (5.3 ± 0.3 %), consistent with an origin by fractional crystallization from a mafic melt with very minor continental crustal contamination. The geochronological and geochemical data suggest that mafic and felsic volcanic rocks of the NVC are genetically closely related to each other. Mafic rocks show a positive trend between $^{87}Sr/^{86}Sr$ and Th, suggesting simultaneous assimilation and fractional crystallization, whereas the felsic rocks are characterized by a flat or slightly negative variation. High $^{87}Sr/^{86}Sr$ gneisses are a potential crustal contaminant of the mafic magmas, but the comparatively low and invariant $^{87}Sr/^{86}Sr$ in the felsic volcanics suggests that these evolved dominantly by fractional crystallization. Mantle-derived basaltic melts, which experienced low degree of crustal assimilation, are proposed to be the parent melt of the felsic volcanics. Geochronological and geochemical results combined with regional geological and geophysical data suggest that bimodal volcanism of the NVC and the CVP, in general, developed in a post-collisional extensional tectonic regime that is caused by ascending asthenosphere, which played a key role during magma genesis.

Keywords Central Anatolia, Turkey · Cappadocia · Niğde · Bimodal volcanism · FC and AFC processes · Post-collisional extensional setting

Introduction

Coeval mafic and felsic volcanism lacking intermediate magma compositions occurs in different geodynamic environments, including continental and back-arc oceanic rift settings (e.g., Duncan et al. 1984; Garland et al. 1995; Deering et al. 2011), within-plate settings and active plate margins (e.g., Coulon et al. 1986; Coward et al. 1987; Hildreth et al. 1991; Frost et al. 1999). The characteristic bimodal series of high-K calc-alkaline to alkaline felsic rocks and transitional to Na-alkaline mafic volcanics commonly forms in extensional late-orogenic to post-collisional tectonic regimes (e.g., Turner et al. 1992; Peccerillo et al. 2003; Bonin 2004; Zhang et al. 2008). The recognition of such bimodal series in collision belts can not only provide important information on magma genesis but are also diagnostic geodynamic tracers for constraining the tectonic evolution of these belts. Two main hypotheses have been proposed to explain the genesis of bimodal magmatism. One states a genetic relationship between mafic (mantle-derived) and felsic rocks through fractional crystallization processes with or without crustal contamination (McCulloch et al. 1994; Gertisser and Keller 2000; Peccerillo et al. 2003; Wang et al. 2004; Lacasse et al. 2007; Mtoro et al. 2009). The mafic and felsic rocks share a common mantle-derived parental magma (e.g., Bonin 2004), and generally exhibit similar geochemical signatures and isotopic ratios, with mafic rocks dominating volumetrically; this is frequently the case for continental flood basalt and oceanic island volcanic provinces (e.g., Garland et al. 1995; Geist et al. 1995). The other hypothesis invokes the genesis of mafic and felsic magmas from different sources, the felsic melts being generated either from the anatexis of crustal country rocks or from partial melting of young underplated basalts (Whalen et al. 1987; Hildreth et al. 1991; Turner et al. 1992; Sage et al. 1996; Frost et al. 2001; Van Wagoner et al. 2002), whereas the mafic rocks are derived directly from the mantle by partial melting. In this case, the mafic and felsic rocks show different trace element and isotopic signatures, indicating crustal sources for the felsic rocks and mantle sources for the mafic rocks, and silicic rocks often dominate volumetrically (Doe et al. 1982; Hildreth et al. 1991; Nash et al. 2006; McCurry and Rodgers 2009).

The late Neogene to Quaternary Cappadocian volcanism in central Anatolia has been interpreted as collision-related associated with amalgamation of the Afro-Arabian and Eurasian plates (e.g., Pasquare et al. 1988; Notsu et al. 1995). However, some recent studies refer to the presence of transitional and alkaline volcanism as connected to an extensional regime (e.g., Dirik and Göncüoğlu; 1996; Toprak 1998; Alıcı Şen et al. 2004; Aydin 2008). It was suggested that the strongly calc-alkaline rocks were derived from a lithospheric mantle source that was metasomatized by previous subduction, whereas the transitional and slightly alkaline volcanic rocks were generated from more depleted magmas (e.g., Aydar et al. 1995; Deniel et al. 1998; Alıcı Şen et al. 2004) or from a metasomatised lithospheric mantle source with variable contributions of an asthenospheric source (Aydin 2008; Gençalioğlu Kuşçu and Geneli 2010; Aydin et al. 2011, 2012). Age and petrogenesis of the young bimodal volcanic rock series in the Cappadocian Volcanic Province (CVP) of central Anatolia have been controversially discussed for a long time due to the limited geochronological and isotopic data. In this paper, we present new geochronological (U–Pb zircon and ^{40}Ar-^{39}Ar amphibole and whole-rock ages) and geochemical data including Sr–Nd–Pb and $\delta^{18}O$ isotopes for the young mafic and felsic volcanic rocks of the Niğde Volcanic Complex (NVC), western CVP, and we evaluate their genetic relationships and geodynamic setting. Quaternary bimodal volcanic rocks in the NVC have ages (ca. 1.1–0.2 Ma) that overlap with the ages of the Erciyes and Acıgöl volcanic fields in the CVP which are ca. 2.5–0.08 and ca. 0.25–0.02 Ma, respectively (Notsu et al. 1995; Kürkçüoğlu et al. 1998; Druitt et al. 1995; Schmitt et al. 2011). Collectively, these volcanic fields exist in a regional post-collisional extensional tectonic regime, most probably related to the presence of hot asthenospheric mantle

beneath the region, as indicated by mantle tomography studies (e.g., Gans et al. 2009; Dilek and Sandvol 2009; Biryol et al. 2011). In this regard, our results allow illuminating the connection between bimodal mafic-felsic magmatism and late Neogene–Quaternary plate dynamics in the eastern Mediterranean region.

Geological background

General geology

Anatolia's complex tectonic evolution within the Alpine-Himalayan framework involves the closure of several branches of the Neotethyan Ocean during the late Mesozoic and Cenozoic (e.g., Şengör and Yılmaz 1981), followed by ongoing collision between the northward-moving Afro-Arabian plates and the relatively stable Eurasian plate in the late Neogene (Şengör et al. 1985; Yılmaz 1993; Okay and Tüysüz 1999; Bozkurt 2001; Dilek 2006). These plate interactions produced complex patterns of subduction which varied in time and space with the geometry of continental plate margins (McKenzie 1972; Şengör and Kidd 1979). Subduction also established a broad volcanic belt ranging from Greece, through Anatolia, into northwestern Iran. This belt is subdivided into several Neogene to Quaternary volcanic provinces which differ in age and composition (Fig. 1a).

The CVP ranks among the best preserved volcanic landscapes of this age worldwide, and the preservation of voluminous volcaniclastic deposits implicates it as one of the most complete examples for the transition from collision to post-collision volcanism in the Alpine-Himalayan belt. It extends NE–SW for a length of ~300 km and a width of ~40–100 km and is associated with two main strike-slip faults, the Tuzgölü Fault Zone (TFZ) and the Ecemiş Fault Zone (EFZ) or central Anatolian Fault Zone (CAFZ) (Fig. 1a, b), that control the overall location of the volcanic centers within the area (Toprak and Göncüoğlu1993; Kocyigit and Beyhan 1998). Most of the late Neogene to Quaternary polygenetic volcanoes in the CVP are aligned NE–SW, parallel to the direction of the EFZ (Fig. 1b), whereas Quaternary monogenetic volcanoes comprising scoria cones with lava flows, domes and maars are fed by dikes injected along the recent fractures of both TFZ and EFZ systems (Toprak 1998). At least 500 monogenetic volcanoes have been identified within the CVP, and based on petrographic and geochemical data, they consist of basalts, trachybasalts, basaltic andesites and rhyolites (Pasquare et al. 1988; Ercan et al. 1992; Aydar et al. 1995; Aydar 1997; Deniel et al. 1998). Detailed geological, geochronological and geochemical descriptions and data for the late Neogene–Quaternary volcanoes and volcaniclastic units in the CVP are presented elsewhere (Innocenti et al. 1975; Besang et al. 1977; Pasquare et al. 1988; Ercan et al. 1992; Göncüoğlu and Toprak 1992; Le Pennec et al. 1994; Aydar and Gourgaud 1998; Temel et al. 1998; Türkecan et al. 2003; Aydin 2008; Gençalioğlu Kuşçu and Geneli 2010; Aydin et al. 2011; Schmitt et al. 2011; Aydar et al. 2012).

Niğde Volcanic Complex (NVC)

The NVC is one of the major Neogene–Quaternary volcanic centers in the western part of the CVP (Fig. 1b). The late Neogene evolution of the NVC initiated with the eruption of extensive andesitic-dacitic lava flows and pyroclastic flow and fall-out deposits, which are associated with the stratovolcanoes such as Hasandağı, Melendiz and Keçiboyduran (Fig. 1b, c). Minor basaltic lava flows and scoria fall-out deposits represent the latest products of the stratovolcanoes in the region. A younger phase of Quaternary bimodal volcanism produced the last volcanic cover of the central Anatolian Crystalline Complex (CACC) and the Niğde Massif (Fig. 1b, c) that consist of two mountainous ranges exposing a basement sequence comprising Precambrian, Paleozoic-Mesozoic metamorphic rocks, Cretaceous supra-subduction zone ophiolitic rocks and Cretaceous granitoids (Göncüoğlu 1986; Whitney and Dilek 1997; Parlak et al. 2002; Köksal and Göncüoğlu 2008; Dilek and Sandvol 2009).

The geology of the volcanic rocks presented here is based on the previous investigations (e.g., Beekman 1966; Göncüoğlu and Toprak 1992; Aydin et al. 2011) which establish the following units for the NVC: (1) Miocene–Pliocene volcaniclastic rocks, (2) late Neogene–Quaternary polygenetic volcanoes, (3) Quaternary domes and cinder cones with related lavas and (4) Quaternary fan to terrace and fluvial-deposits (Fig. 1c). The NVC comprises seven separate volcanic units, which are, from oldest to youngest, Keçikalesi, Tepeköy, Çınarlı, Kızılçin, Melendiz, Keçiboyduran and Hasandağı and a number of monogenetic vents with related mafic and felsic lavas and pyroclastic deposits of Quaternary age (i.e., around Keçiboyduran-Hasandağı and Göllüdağ; Fig. 1b, c). Ercan et al. (1992), Notsu et al. (1995), Aydar (1997), Deniel et al. (1998) and Alıcı Şen et al. (2004) investigated the geochemistry and petrology of the samples from many monogenetic cones and related lava flows around Keçikalesi, Hasandağı and Keçiboyduran (Fig. 1c). According to these geochemical analyses, the samples were classified as basalts, basaltic andesites and minor trachybasalts. K/Ar geochronology of the monogenetic cones in this region yielded ages from ca. 1.15 ± 0.76 to ca. 0.06 ± 0.01 Ma (Ercan et al. 1992). Monogenetic volcanoes around the Keçiboyduran, Göllüdağ and Kızılçin toward the Acıgöl area (Fig. 1c) are Quaternary in age and include scoria lapilli fallout deposits associated with lava

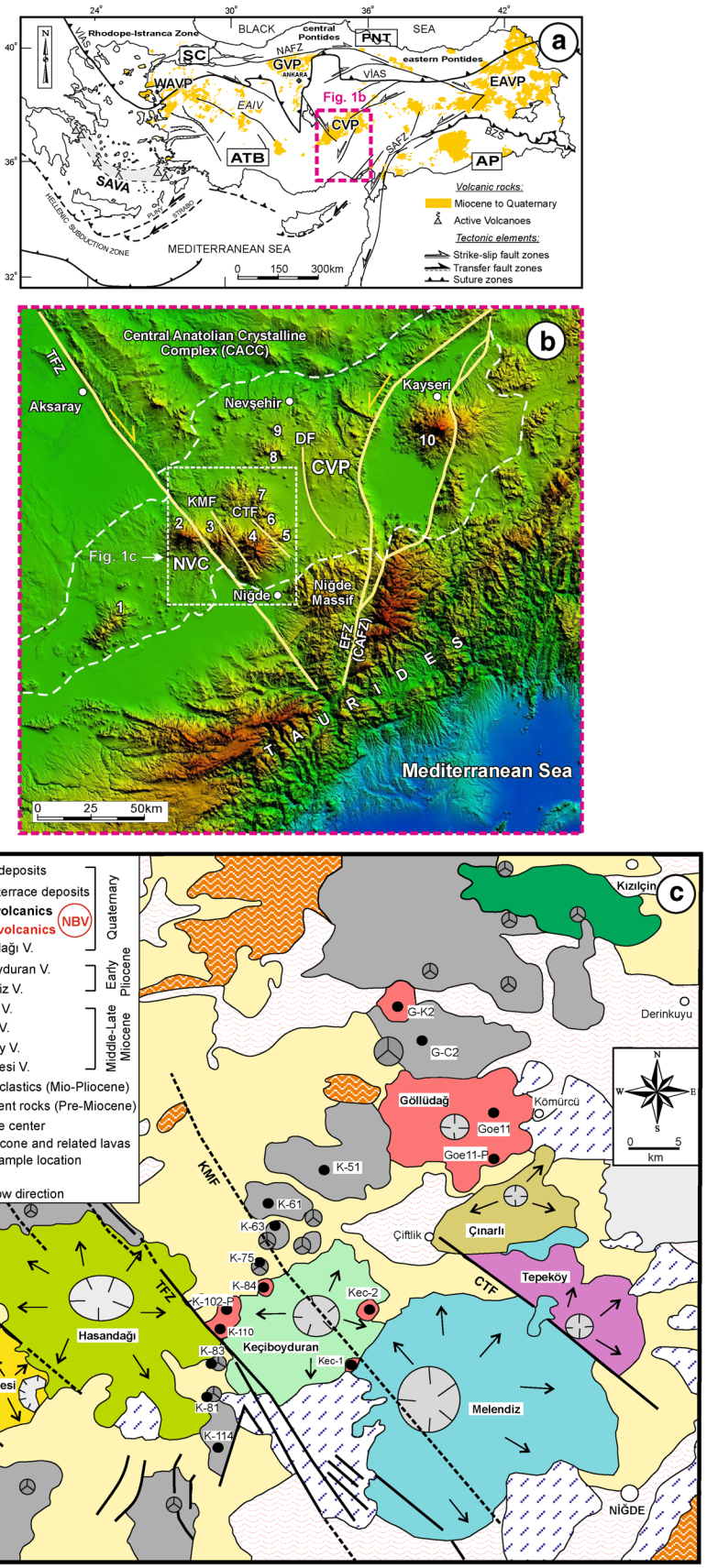

Fig. 1 **a** Regional tectonic map of Anatolia (Turkey) with main blocks [modified from Okay and Tüysüz (1999)] showing the distribution of main Neogene–Quaternary volcanic provinces (modified from Geological Map of Turkey 2002; 1:500,000) with location of the study area. *SC* Sakarya continent, *PNT* Pontides, *ATB* Anatolide-Tauride block, *AP* Arabian platform, *SAVA* South Aegean volcanic arc, *WAVP* Western Anatolian volcanic province, *GVP* Galatian volcanic province, *CVP* Cappadocian volcanic province, *EAVP* Eastern Anatolian volcanic province, *NAFZ* North Anatolian Fault Zone, *SAFZ* South Anatolian Fault Zone, *VIAS* Vardar-İzmir-Ankara suture, *BZS* Bitlis-Zagros suture. **b** Simplified map showing Neogene–Quaternary major structural elements and main volcanic centers of the CVP with the study area (*NVC* Niğde Volcanic Complex) over topography of central Anatolia and Taurides derived from 90-m SRTM digital elevation model. *TFZ* Tuzgölü fault zone, *EFZ (or CAFZ)* Ecemiş (or central Anatolian) fault zone, *KMF* Keçiboyduran and Melendiz fault, *CTF* Çınarlı-Tepeköy fault, *DF* Derinkuyu fault. Volcanic centers (from Toprak 1998); *1* Karacadağ, *2* Hasandağ, *3* Keçiboyduran, *4* Melendiz, *5* Tepeköy, *6* Çınarlı, *7* Göllüdağ, *8* Kızılçin, *9* Acıgöl, *10* Erciyes. **c** Simplified geological map of the NVC with the major faults (modified from Göncüoğlu and Toprak 1992) and main volcanic centers, which also show the distribution of Quaternary Niğde bimodal volcanic rocks (NBV) and sample locations

flows and domes with pumice lapilli fall-out and surge deposits, which are mainly basaltic and rhyolitic in composition, respectively (Batum 1978; Bigazzi et al. 1993). These basaltic and rhyolitic rock samples represent the youngest volcanic products of the NVC and form a bimodal magma suite.

Analytical methods

Whole-rock geochemical analyses

Eight mafic and eight felsic representative rock samples, visibly free of alteration, were taken from scoria lapilli fallout deposits associated with lava flows and domes with pumice lapilli fall-out and surge deposits around the Keçiboyduran and Göllüdağ volcanoes in the NVC from the CVP (sampling localities and GPS coordinates are shown in Fig. 1c; Table 1, respectively). Following petrographic examination, samples were crushed in a steel jaw crusher and then powdered in an agate mill to a grain size of <0.074 mm. Powder aliquots for bulk-rock analyses were prepared by quarter reduction of splits from the samples weighing 1–2 kg. The major, trace and rare earth element contents (Table 1) were determined at the commercial ACME Laboratories Ltd. in Vancouver (Canada). Major elements were measured by ICP-AES after fusion with $LiBO_2/LiB_4O_7$. Detection limits were ~0.001–0.04 %. For trace and rare earth element analyses, 0.2 g of sample powder and 1.5 g of $LiBO_2/LiB_4O_7$ flux were mixed in a graphite crucible and subsequently heated to 1,050 °C for 15 min. The molten sample was then dissolved in 5 % HNO_3. The sample solutions were aspirated into an ICP-MS (Perkin–Elmer Elan 600). The detection limits ranged from 0.01 to 0.5 ppm. Measurements were taken using the control standard STD SO-17 which was calibrated against 38 Certified Reference materials including CANMET SY-4 and USGS AGV-1, G-2, GSP-2 and W-2.

Sr–Nd–Pb isotope analyses

For Sr–Nd isotope analyses, whole-rock powders were dissolved in 52 % HF for 4 days at 140 °C on a hot plate. Digested samples were dried and redissolved in 6 N HCL, dried again and redissolved in 2.5 N HCl. Sr and the light rare earth elements were separated by standard ion exchange chromatography with a 5-ml resin bed of AG 50 W-X12 (0.074–0.037 mm). Nd was separated from the other rare earth elements on quartz columns using 1.7-ml Teflon powder coated with HDEHP, di (2-ethylhexyl) orthophosphoric acid, as the cation exchange medium. Isotopic data were obtained in static mode on a Finnigan MAT 262 mass spectrometer at the Department of Geosciences, Tübingen University. The Sr fraction was dissolved in 1–2 µl of 2.5 mol HCl and loaded with a Ta-activator onto a previously outgassed W single filament and measured at 1,300–1,400 °C. Nd (as phosphate) was dissolved in 1 µl ultrapure H_2O and was measured as Nd^+ on a Re double filament configuration at temperatures between 1,700 and 1,800 °C. The $^{143}Nd/^{144}Nd$ ratios were normalized to $^{146}Nd/^{144}Nd = 0.7219$ and the $^{87}Sr/^{86}Sr$ isotope ratios to $^{86}Sr/^{88}Sr = 0.1194$. Analyses of five different loads of La Jolla standard gave $^{143}Nd/^{144}Nd$ ratios of 0.511844 ± 0.000008 ($2\sigma_m$), and fifteen analyses of the NBS 987 Sr standard yielded a $^{87}Sr/^{86}Sr$-ratio of 0.710223 ± 0.000022 ($2\sigma_m$) in good agreement with the certified values. Total procedural blanks (chemistry and loading) were better than 190 pg for Sr and 90 pg for Nd. εNd values were calculated using present-day CHUR values of 0.1967 for $^{147}Sm/^{144}Nd$ and 0.512638 for $^{143}Nd/^{144}Nd$. Depleted mantle Nd model ages (T_{DM}) were calculated with depleted present-day parameters $^{143}Nd/^{144}Nd = 0.513151$ and $^{147}Sm/^{144}Nd = 0.219$.

Separation and purification of Pb was achieved on Teflon columns with a 100-µl (separation) and 40-µl bed (cleaning) of Bio-Rad AG1-X8 (0.149-0.074 mm) anion exchange resin using a HBr–HCl ion exchange procedure. Isotopic measurements were taken by thermal ionization mass spectrometry on a Finnigan MAT 262 mass spectrometer at Tübingen University. Pb was loaded with a Si-gel onto a Re filament and measured at ~1,300 °C in single-filament mode. A factor of 1 ‰ per mass unit for instrumental mass fractionation was applied to the Pb analyses, using NBS SRM 981 as reference material. Total procedural blanks during the measurement period were between 15 and 30 pg for Pb.

Zircon oxygen isotope analyses

Felsic whole-rock samples (pumice or lava) were crushed and sieved, and zircon crystals separated from the washed <250 µm size fraction by gravitational settling in heavy liquids. Oxygen isotopes were analyzed using the UCLA CAMECA ims 1270 in multi-collection mode following techniques described in Trail et al. (2007). Instrumental mass fractionation was corrected by analyzing standard zircon AS3 with $\delta^{18}O_{SMOW} = 5.34$ ‰ (Trail et al. 2007). Individual spots have uncertainties between ~0.3 and 0.6 ‰ (1 standard deviation) based on the external reproducibility of AS3 standard zircon analyses.

Geochronological analyses

U–Pb analyses

U–Pb isotopes in zircon were analyzed with the UCLA CAMECA ims 1,270 using methods described in Schmitt

Table 1 Whole-rock major oxide and trace element analyses of the Niğde bimodal volcanic rocks

Location	Göllüdağ				Keçiboyduran											
Sample	Goell	Goell-P	G-K2	G-C2	K-51	K-61	K-75	K-83	K-63	K-81	K114	K-84	K110	KEC-1	KEC-2	K102P
Rock type	Ry-lava	Ry-pumice	Ry-lava	B-lava	B-lava	B-lava	B-scoria	B-scoria	TB-lava	TB-lava	TB-lava	Ry-lava	Ry-lava	Ry-pumice	Ry-pumice	Ry-pumice
Longitude	38°16′36″	38°13′51″	38°22′25″	38°20′35″	38°11′19″	38°11′52″	38°00′08″	38°05′08″	38°10′41″	38°04′18″	38°03′34″	38°06′42″	38°06′18″	38°00′57″	38°10′33″	38°07′05″
Latitude	34°33′15″	34°32′29″	34°31′29″	34°31′50″	34°23′35″	34°21′19″	34°20′37″	34°17′39″	34°21′20″	34°17′30″	34°17′02″	34°17′25″	34°17′57″	34°23′34″	34°25′19″	34°16′39″
Altitude (m)	1,641	1,690	1,416	1,373	1,584	1,415	1,638	1,647	1,524	1,463	1,330	1,935	1,977	1,402	1,637	1,896
Age (Ka)	1,089	899			654*				224*	490*		447	530*	438	349	339
Sio_2	74.2	71.1	74.4	49.3	50.9	49.0	50.0	50.7	50.2	51.8	51.9	71.8	70.7	72.8	69.5	67.8
Al_2o_3	13.3	13.0	12.8	18.4	16.4	18.0	16.7	16.3	16.9	18.6	18.4	14.9	14.5	12.7	14.3	15.0
$Fe_2o_3^{(t)}$	0.86	1.38	0.91	9.79	8.80	9.62	8.44	7.98	8.66	7.93	8.17	1.91	1.85	0.68	2.02	2.78
Mgo	0.07	0.16	0.05	6.12	7.22	6.75	5.55	7.25	7.00	5.27	4.74	0.66	0.64	0.13	0.77	1.13
Cao	0.38	0.81	0.48	9.90	9.38	9.81	10.3	10.2	8.34	8.39	8.47	2.09	2.08	0.61	2.25	2.99
Na_2o	3.84	3.84	3.80	3.76	3.64	3.88	3.61	3.14	4.17	4.07	4.02	4.40	4.12	3.14	3.77	4.03
K_2o	4.43	4.47	4.85	0.55	1.11	0.57	1.59	1.32	1.38	1.26	1.39	3.17	3.26	4.85	3.45	3.01
Tio_2	0.07	0.09	0.06	1.49	1.29	1.56	1.19	1.07	1.60	1.33	1.32	0.28	0.26	0.10	0.29	0.39
P_2o_5	0.02	0.03	0.01	0.25	0.38	0.25	0.53	0.33	0.50	0.45	0.44	0.08	0.08	0.04	0.08	0.10
Mno	0.07	0.06	0.05	0.17	0.16	0.17	0.15	0.13	0.15	0.13	0.13	0.06	0.06	0.05	0.06	0.06
Cr_2o_3	0.00	0.00	0.00	0.01	0.04	0.01	0.01	0.03	0.02	0.00	0.00	0.00	0.00	0.00	0.00	0.00
LoI	3.63	3.63	2.60	0.20	0.40	0.10	1.60	1.20	0.80	0.60	0.70	0.60	2.40	4.80	3.40	2.60
Total	100.8	98.6	100.0	99.9	99.7	99.7	99.6	99.7	99.7	99.7	99.7	99.9	99.9	99.9	99.9	99.9
Mg#	13	17	9	53	62	56	54	62	59	54	51	38	38	25	40	42
Na/K	0.9	0.9	0.8	6.8	3.3	6.8	2.3	2.4	3.0	3.2	2.9	1.4	1.3	0.6	1.1	1.3
Cs	8.0	15.0	7.2	0.2	0.2	0.1	3.8	0.6	0.4	0.9	0.2	3.8	4.1	5.1	4.0	4.0
Rb	183	163	179	7	17	8	44	28	22	23	26	93	107	117	112	107
Ba	89	395	195	200	367	155	617	458	329	432	426	745	702	799	668	630
Sr	8	72	16	502	648	508	947	1,007	656	766	760	229	221	65	217	270
Pb	20	21	0.2	0.9	3.7	0.5	2.1	1.1	0.8	2.2	5.4	0.8	0.8	0.4	0.5	1.2
Th	21.0	21.0	22.7	1.6	4.2	1.9	8.6	8.3	4.3	6.0	6.7	14.5	14.2	12.1	13.6	14.0
U	7.0	4.0	8.4	0.3	1.0	0.4	1.7	1.8	0.9	1.3	1.5	4.4	4.3	5.3	4.6	4.0
Zr	80	134	75	133	163	137	162	126	198	137	139	134	129	49	117	174
Hf	19	17.0	2.5	2.8	3.6	3.3	4.2	3.4	4.4	3.5	3.0	4.0	3.6	2.2	3.0	4.5
Ta	nd	nd	nd	0.5	0.8	0.4	0.8	0.5	1.1	0.9	0.9	1.0	1.0	1.3	1.0	0.8
Y	16	17.0	21.1	27.7	26.9	26.0	22.2	20.1	25.1	20.9	21.0	14.1	13.9	12.2	13.7	14.4

Table 1 continued

Location	Göllüdağ				Keçiboyduran											
Sample	Goell	Goell-P	G-K2	G-C2	K-51	K-61	K-75	K-83	K-63	K-81	K114	K-84	K110	KEC-1	KEC-2	K102P
Rock type	Ry-lava	Ry-pum-ice	Ry-lava	B-lava	B-lava	B-lava	B-scoria	B-scoria	TB-lava	TB-lava	TB-lava	Ry-lava	Ry-lava	Ry-pum-ice	Ry-pum-ice	Ry-pumice
Longitude	38°16′36″	38°13′51″	38°22′25″	38°20′35″	38°11′19″	38°11′52″	38°00′08″	38°05′08″	38°10′41″	38°04′18″	38°03′34″	38°06′42″	38°06′18″	38°00′57″	38°10′33″	38°07′05″
Latitude	34°33′15″	34°32′29″	34°31′29″	34°31′50″	34°23′35″	34°21′19″	34°20′37″	34°17′39″	34°21′20″	34°17′30″	34°17′02″	34°17′25″	34°17′57″	34°23′34″	34°25′19″	34°16′39″
Altitude (m)	1,641	1,690	1,416	1,373	1,584	1,415	1,638	1,647	1,524	1,463	1,330	1,935	1,977	1,402	1,637	1,896
Age (Ka)	1,089	899			654*				224*	490*		447	530*	438	349	339
Nb	12	14.0	6.2	9.8	13.2	7.1	18.1	9.9	16.6	16.0	15.5	12.6	11.5	9.5	11.7	10.6
Sc	3	4	2	24	26	27	23	26	20	18	18	4	3	2	4	5
Cr	nd	nd	nd	292.4	584.8	146.2	2,339.2	1,754.4	1,169.6	877.2	1,023.4	877.2	3,508.8	7,017.6	4,970.8	3,801.2
Ni	nd	nd	nd	38.1	96.4	39.6	26.3	76.3	103.3	54.5	58.0	2.5	nd	2.0	nd	nd
Co	nd	nd	nd	35.5	37.0	40.0	33.7	31.2	30.5	26.1	28.4	3.8	3.0	0.9	6.0	17.6
V	6	9	5	195	216	210	177	209	153	158	175	12	18	8	24	38
W	nd	nd	nd	0.3	0.5	0.5	0.7	0.5	0.6	0.5	0.5	2.1	1.6	1.9	1.8	1.6
Ga	35.0	38.0	14.5	18.5	16.7	16.7	17.6	16.2	15.8	17.4	18.0	15.0	13.7	12.5	14.9	14.8
Zn	0.0	8.0	2.0	47.0	49.0	48.0	30.0	34.0	49.0	48.0	37.0	10.0	8.0	5.0	8.0	7.0
Cu	28.0	20.0	1.2	21.4	43.8	29.8	96.4	44.1	28.3	15.1	15.8	2.0	2.1	4.1	2.1	15.0
La	19.0	24.0	24.4	13.9	28.3	14.1	44.4	31.3	25.3	30.7	30.0	29.3	28.2	15.7	24.2	28.6
Ce	62.0	81.0	46.9	32.2	57.6	32.5	90.6	65.1	54.8	61.7	61.0	52.9	50.6	31.0	45.1	51.4
Pr	nd	nd	4.4	4.0	6.4	4.2	10.1	7.5	6.4	6.6	6.6	5.2	4.9	3.1	4.4	5.0
Nd	12	13	14.3	17.7	26.6	18.3	39.3	29	25.7	24.8	23.9	17.2	15.2	10.2	13.3	16.1
Sm	2.60	3.20	2.60	4.10	4.96	4.15	6.56	5.08	5.18	4.36	4.41	2.71	2.58	1.75	2.34	2.73
Eu	0.10	0.30	0.16	1.42	1.56	1.44	1.77	1.46	1.56	1.37	1.32	0.62	0.59	0.31	0.58	0.66
Gd	6.00	4.00	2.44	4.45	4.88	4.58	5.19	4.11	4.88	3.99	4.28	2.21	2.21	1.45	2.21	2.46
Tb	nd	nd	0.51	0.83	0.85	0.81	0.80	0.67	0.83	0.66	0.66	0.41	0.37	0.32	0.37	0.39
Dy	nd	nd	2.97	4.69	4.59	4.51	4.14	3.38	4.42	3.79	3.62	2.13	2.16	1.95	2.08	2.27
Ho	nd	nd	0.60	0.96	0.95	0.89	0.76	0.68	0.83	0.71	0.72	0.45	0.41	0.36	0.42	0.45
Er	nd	nd	1.91	2.71	2.86	2.85	2.21	2.03	2.65	2.08	2.08	1.41	1.30	1.22	1.33	1.32
Tm	nd	nd	0.32	0.37	0.43	0.42	0.34	0.28	0.40	0.31	0.29	0.22	0.22	0.18	0.21	0.22
Yb	2.90	2.70	2.13	2.45	2.71	2.53	1.99	1.74	2.40	1.84	1.86	1.42	1.51	1.22	1.42	1.43
Lu	0.50	0.50	0.36	0.39	0.40	0.38	0.31	0.27	0.35	0.29	0.28	0.22	0.23	0.19	0.45	0.25
Nb/Ta				20	17	18	23	20	15	18	17	13	12	10	12	13
Nb/La	0.6	0.6	0.3	0.4	0.5	0.5	0.4	0.3	0.7	0.5	0.5	0.4	0.4	0.6	0.5	0.4
Zr/Sm	31	42	29	32	33	33	25	25	38	31	31	49	50	28	50	64

Table 1 continued

Location	Göllüdağ				Keçiboyduran											
Sample	Goell	Goell-P	G-K2	G-C2	K-51	K-61	K-75	K-83	K-63	K-81	K114	K-84	K110	KEC-1	KEC-2	K102P
Rock type	Ry-lava	Ry-pum-ice	Ry-lava	B-lava	B-lava	B-lava	B-scoria	B-scoria	TB-lava	TB-lava	TB-lava	Ry-lava	Ry-lava	Ry-pum-ice	Ry-pum-ice	Ry-pumice
Longitude	38°16′36″	38°13′51″	38°22′25″	38°20′35″	38°11′19″	38°11′52″	38°00′08″	38°05′08″	38°10′41″	38°04′18″	38°03′34″	38°06′42″	38°06′18″	38°00′57″	38°10′33″	38°07′05″
Latitude	34°33′15″	34°32′29″	34°31′29″	34°31′50″	34°23′35″	34°21′19″	34°20′37″	34°17′39″	34°21′20″	34°17′30″	34°17′02″	34°17′25″	34°17′57″	34°23′34″	34°25′19″	34°16′39″
Altitude (m)	1,641	1,690	1,416	1,373	1,584	1,415	1,638	1,647	1,524	1,463	1,330	1,935	1,977	1,402	1,637	1,896
Age (Ka)	1,089	899			654*				224*	490*		447	530*	438	349	339
Sr/Y	1	4	1	18	24	20	43	50	26	37	36	16	16	5	16	19
La/Yb	7	9	11	6	10	6	22	18	11	17	16	21	19	13	17	20

* Radiometric data were obtained by the ^{40} Ar/^{39}Ar incremental heating method and the others are U–Pb zircon ages, Mg# = (molar Mg/[Mg + Fe)], *nd* not detected, *Ry* Rhyolite, *B* Basalt, *TB* Trachybasalt

et al. (2003). U–Pb ages are relative to AS3 secular equilibrium standard (1,099 Ma; Paces and Miller 1993) mounted adjacent to the unknowns. Analytical reproducibility of ^{206}Pb/^{238}U ages is estimated from replicate analyses of AS3 and varied between 1.3 and 2.2 % (1 standard deviation of 10 and 23 replicates, respectively). Ages are determined from linear regression of the data uncorrected for common Pb, with the intersection of the regression line with concordia (modified to account for initial ^{230}Th disequilibrium with corresponding to a zircon–melt partitioning ratio $D_{Th}/D_U = 0.2$). We report all data including those with comparatively low radiogenic Pb. Although low radiogenic zircons have poor age resolution, these analyses aid in defining the slope of the regression line. Where data spread was limited, a common Pb composition of ^{207}Pb/^{206}Pb = 0.823 corresponding to Southern California anthropogenic Pb (Sañudo-Wilhelmy and Flegal 1994) as a surface contaminant was assumed. Uranium concentrations in zircon were estimated from standard zircon 91,500 (U = 81 ppm; Liu et al. 2010) to within an approximate uncertainty of 10 % (relative error).

Ar–Ar analyses

The incremental heating ^{40}Ar/^{39}Ar age determinations were performed on crystalline 300–600-μm amphibole separates and whole-rock samples using a continuous, 10 W CO_2 laser probe connected to a MAP-215/50 mass spectrometer at Oregon State University, USA. Fresh samples were reduced in a small jaw crusher with alumina surfaces, followed by sieving to obtain the 300–600-μm size fractions. The separates were further cleaned by mild acid leaching (1 N HNO_3 for ~20 min) in an ultrasonic bath that was heated to approximately 50 °C. Finally, the leached separates were washed in ultraclean water and dried in an oven (~40 °C). The samples were wrapped in Cu foil, loaded in evacuated quartz tubes, alternating with packages of FCT-3 biotite monitor standard and irradiated for 6 h in a TRIGA reactor ICIT facility. Values of the irradiation parameter *J* for individual sample positions were calculated by polynomial interpolation between the measured monitors. Estimated uncertainties for *J* are between 0.2 and 0.3 %. Then, 80 mg of irradiated samples were loaded into Cu planchettes, which were then pumped within a sample chamber fitted with a ZnS window transparent to the CO_2 laser wavelength. Software allowed for scanning across samples in a preset pattern with a defocused beam to evenly heat the material. Gas cleanup was accomplished with a series of Zr-Al getters. All ^{40}Ar/^{39}Ar ages were calculated using the corrected decay constant of $5.530 \pm 0.097 \times 10^{-10}$ 1/a (2σ) (Steiger and Jäger 1977) as reported by (Min et al. 2000). Detailed descriptions of the analytical procedure and age calculations can be found in Koppers (2002 and references therein) and at http://earthref.org/tools/ararcalc.htm.

Fig. 2 Macroscopic views and typical features of the Niğde bimodal volcanic rocks. **a** Close-up of flow banding in Göllüdağ rhyolites (Sample no: Goell). **b** Göllüdağ pyroclastic fall-out and surge deposits in outcrop (Sample no: Goell-P). **c** Field relations between basaltic cinder cone (Sample no: K-75) and related lava flow (Sample no: K-63) around Keçiboyduran stratovolcano. **d** Granitic xenolith in alkaline basalt (Sample no: K-114). Photomicrographs showing mineral assemblages and textural characteristics of the rhyolites (**e**) and olivine basalts (**f**–**h**). *Pl* plagioclase, *Amp* amphibole, *Ol* olivine, *Cpx* clinopyroxene, *Fe* Fe–Ti oxides, *Q* Quartz as a xenocryst

Results

Petrography

The Quaternary volcanic units observed in the Göllüdağ dome and around Keçiboyduran stratovolcanoes are represented by (1) felsic volcanics consisting of mostly rhyolitic lavas with flow banding (Fig. 2a) and pumice lapilli fall-out and surge deposits (Fig. 2b) and (2) mafic volcanics consisting of aphanitic and massive basaltic or basaltic andesitic lava flows with some amygdales and scoria lapilli fall-out deposits related to cinder cones (Fig. 2c). Also, the basaltic lavas sometimes contain granitic xenoliths (Fig. 2d). The rhyolitic rocks of Keçiboyduran generally have porphyritic texture with a glassy dark matrix and cryptocrystalline minerals, mainly unzoned plagioclase, hornblende, minor quartz and accessory zircon (Fig. 2e), whereas Göllüdağ rhyolites have plagioclase phenocrysts which display visible oscillatory zoning (Fig. 2f), hornblende microlites and accessory zircon. The mafic volcanics show an

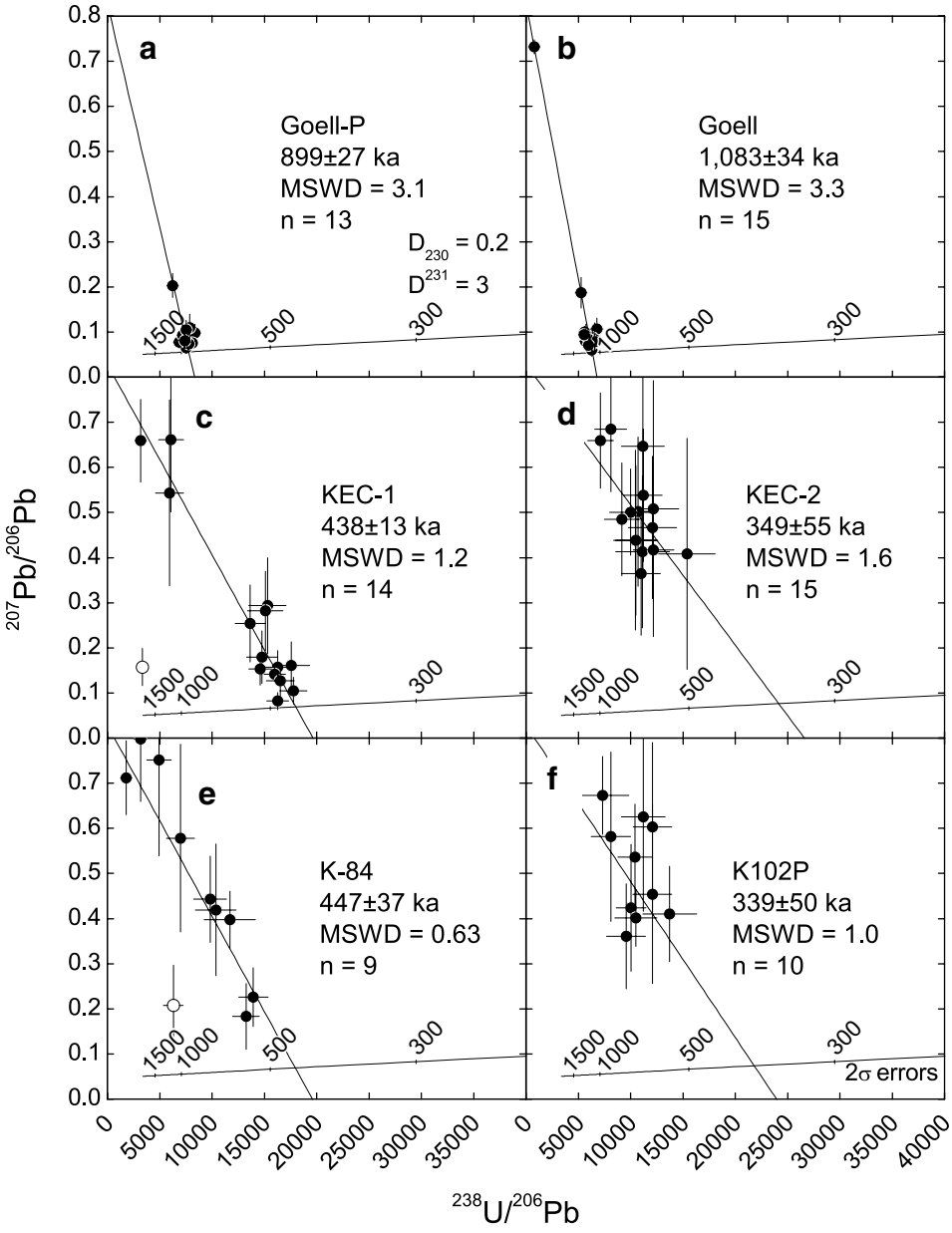

Fig. 3 Ion microprobe U–Pb zircon age results from felsic volcanic products of the NVC in a $^{207}Pb/^{206}Pb$ versus $^{238}U/^{206}Pb$ diagram. Ages are for fixed-intercept regression assuming common $^{207}Pb/^{206}Pb = 0.823$ (Sañudo-Wilhelmy and Flegal 1994). *Open symbol* data point excluded from regression

intergranular texture and contain subhedral phenocrysts of olivine, clinopyroxene and euhedral plagioclase, which are commonly embedded in a cryptocrystalline mafic matrix with some amygdales (Fig. 2g). Quartz xenocrysts are rarely observed in the matrix of mafic rocks and also surrounded by rims consisting of the fine-grained clinopyroxene and olivine (Fig. 2h).

Radiometric ages

U–Pb zircon ages

Zircon crystals from Göllüdağ rhyolites have high U (average 5,400 ± 2,200 ppm; 2 standard deviation), and typically high radiogenic yields (i.e., they generally plot close to concordia in Fig. 3). Average disequilibrium-corrected regression ages range from 1,083 ± 34 ka (Goell) to 899 ± 27 ka (Goell-P) (Table 3, Online Resource 1). The moderately elevated mean squares of weighted deviates (MSWD) suggest some minor age heterogeneity and protracted crystal residence times typical for silicic magma reservoirs (Reid et al. 1997; Brown and Fletcher 1999; Vazquez and Reid 2004; Bachmann et al. 2007; Simon et al. 2008; Wotzlaw et al. 2013) or possibly uncertainties in the disequilibrium correction that are unaccounted for by the error propagation.

Zircons from the two southeastern Keçiboyduran rhyolites have distinct U abundances (KEC-1 = 2,500 ± 2,400 ppm; KEC-2 = 400 ± 90 ppm), resulting in variable spread

on the concordia diagram (Fig. 3). Average disequilibrium-corrected concordia intercept ages are much younger than those for Göllüdağ (KEC-1 = 438 ± 13 ka; KEC-2 = 345 ± 55 ka; Table 3, Online Resource 1) with MSWD values close to unity suggesting a homogeneous age population. The exception is one crystal in KEC-1 which yielded an older age of ~1.75 Ma. The two northwestern Keçiboyduran rhyolites on average have zircon crystals with low U (K-102P = 300 ± 90 ppm; K-84 = 410 ± 360 ppm), similar to those in sample KEC-2. Their disequilibrium-corrected zircon ages are equivalent to those of southeastern Keçiboyduran rhyolites, with K-102P = 339 ± 50 ka and K-84 = 447 ± 36 ka (Table 3, Online Resource 1). Only one slightly older zircon crystal is present with a $^{206}Pb/^{238}U$ age of ~900 ka which was excluded from the regression. The Keçiboyduran zircon age averages fall within a ca. 100 ka age window which is just resolved at the 2σ uncertainty level, but there is a clear temporal gap of ca. 450 ka between rhyolite eruptions from the older Göllüdağ and the younger Keçiboyduran centers.

Ar–Ar amphibole and whole-rock ages

The radiometric data were obtained by the $^{40}Ar/^{39}Ar$ incremental heating method (Table 4, Online Resource 2). Whole-rock ages of mafic samples (K-51, K-63 and K-81) from the basaltic lavas associated with cinder cones around the Göllüdağ and Keçiboyduran yielded weighted mean plateau ages (WMPAs) of 654 ± 24, 224 ± 21 and 490 ± 47 ka (Fig. 4; Table 4, Online Resource 2). The WMPAs comprise four steps and 65 % of the released ^{39}Ar. Hornblende separates from rhyolitic lava sample K110 located between Keçiboyduran and Hasandağı stratovolcanoes (Fig. 1c) yielded a weighted mean plateau age of 530 ± 50 ka (Fig. 4). In two cases, the total fusion ages (TFAs) are indistinguishable from the WMPAs indicating that there is little disturbance in the ^{40}Ar distribution (Fig. 4).

Whole-rock geochemistry

Whole-rock silica contents in the NVC felsic volcanic rocks are between 67.8 and 74.2 wt% (Table 1; Fig. 5a, b). SiO_2 contents of the mafic samples vary within a very narrow range (49.4–51.9 wt%), and their Na_2O/K_2O ratios (2.3–6.8) are higher than those for felsic samples (0.6–1.4), indicating a sodic tendency (Table 1). Magnesium numbers, Mg# (molar Mg/[Mg + Fe)], of the mafic rocks vary between 62 and 51, whereas Mg# of felsic rocks is >42 (Table 1). The felsic rocks plot within the dacite and mostly rhyolite fields of the total alkali-silica diagram

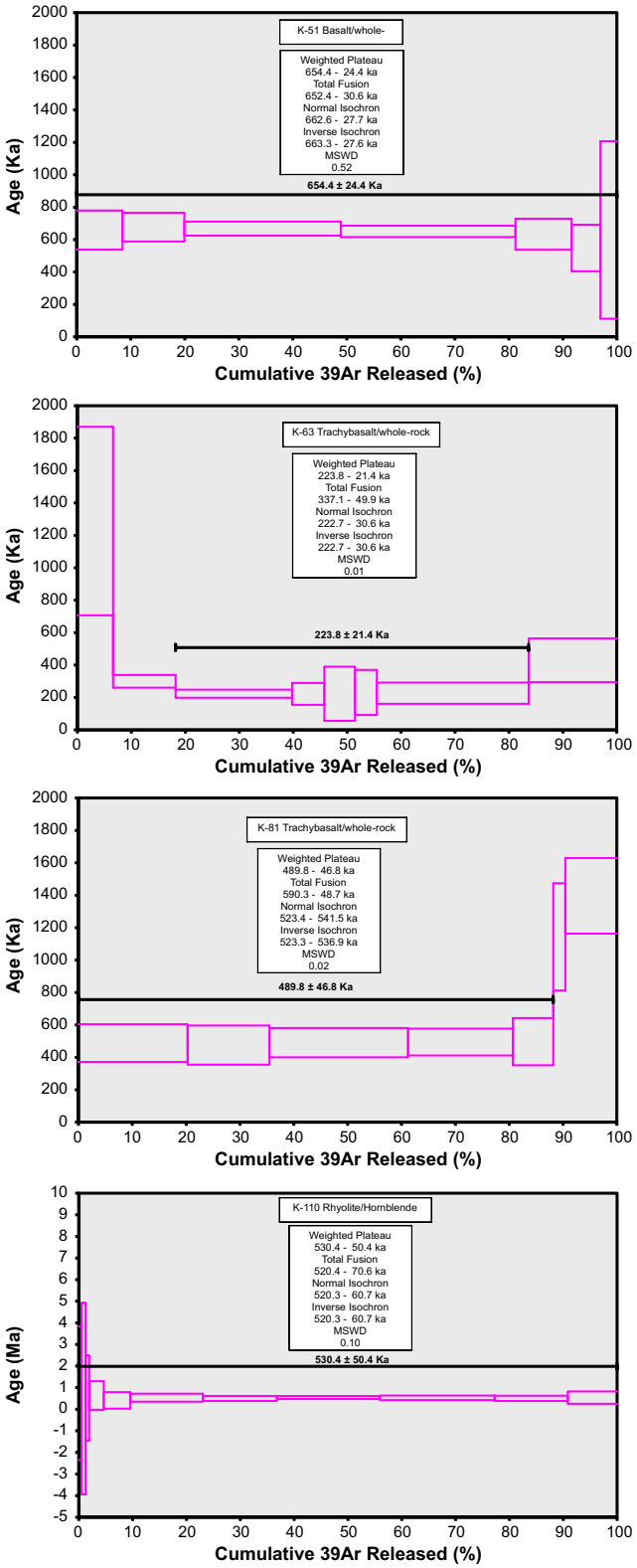

Fig. 4 Plateau ages of basaltic whole rocks and an amphibole of the felsic rocks from the NVC obtained by the $^{40}Ar/^{39}Ar$ stepwise heating technique

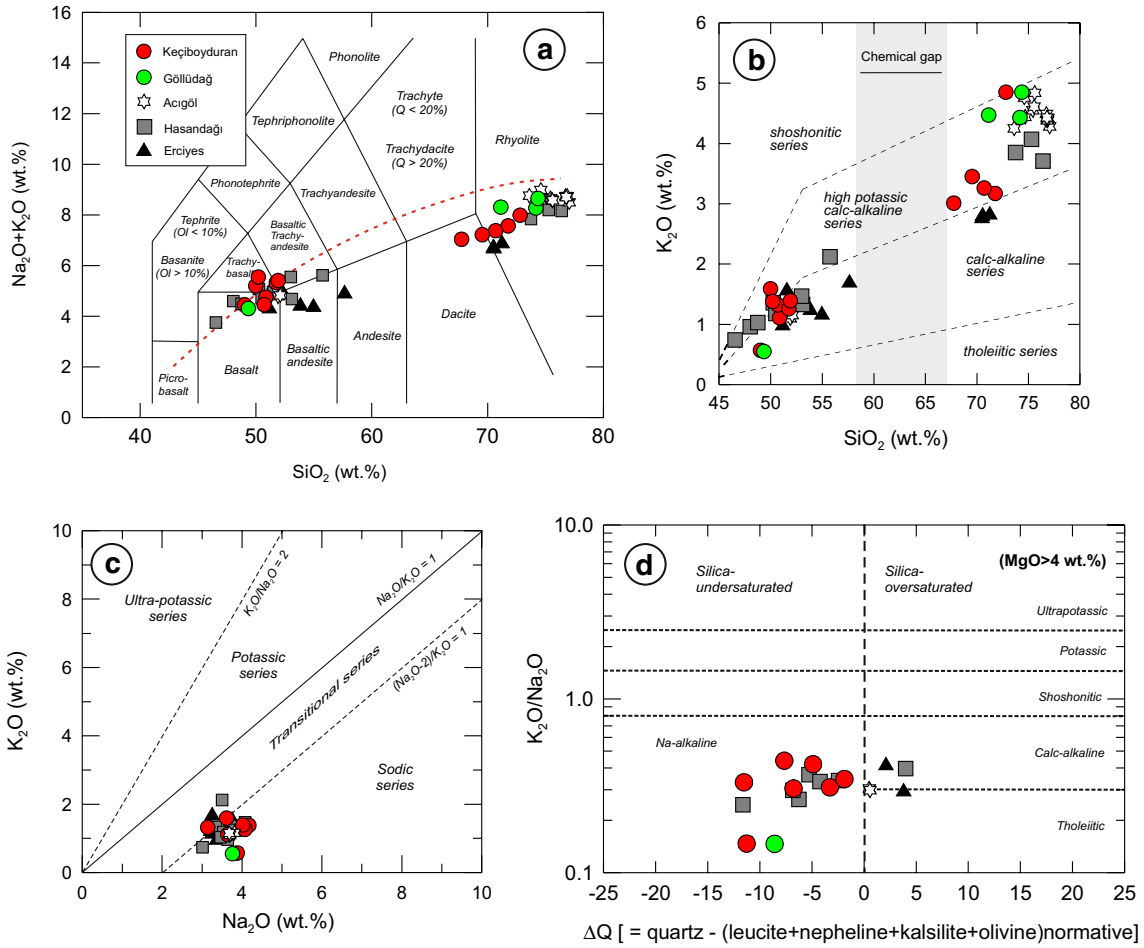

Fig. 5 **a** Total alkali versus silica (TAS) diagram (after Le Maitre 2002) of Niğde bimodal volcanic rocks. *Dashed line* separates alkaline and sub-alkaline compositions. Data from other Pliocene–Quaternary volcanic complexes of the CVP are plotted for comparison. Acıgöl (Siebel et al. 2011); Hasandağı (Deniel et al. 1998); Erciyes (Kürkçüoğlu et al. 1998). **b** K_2O versus SiO_2 diagram for Niğde bimodal rocks with lines separating tholoiitic, calc-alkaline, high-K calc-alkaline and shoshonitic series of Peccerillo and Taylor (1976). **c** K_2O versus Na_2O diagram (from Le Maitre 2002) and **d** ΔQ versus K_2O/Na_2O classification diagram (from Perini et al. 2004) for the mafic samples with MgO > 4 wt%

(from Le Maitre 2002), whereas the mafic samples are classified as basalt, basaltic andesite and trachybasalt (Fig. 5a). The compositional bimodality of the NVC samples is similar to that of the Acıgöl, Hasandağı and Erciyes volcanic complexes within the CVP (Fig. 5a, d). In the K_2O versus SiO_2 diagram (Peccerillo and Taylor 1976), the samples plot along a calc-alkaline differentiation trend with medium- to high-K characteristics (Fig. 5a, b) and K_2O versus Na_2O and K_2O/Na_2O versus ΔQ [= quartz − (leucite + nepheline + kalsilite + olivine)$_{normative}$] diagrams (from Perini et al. 2004) indicate a transitional to Na-alkaline character (silica saturated to silica-undersaturated) for the mafic samples which are Ne-normative (Fig. 5c, d).

Selected major (MgO, Fe_2O_3, TiO_2, CaO, Al_2O_3, P_2O_5) and trace elements (Zr, Rb and Sr) plotted against SiO_2 underline the compositional bimodality of the NVC rocks (Fig. 6). Mafic and felsic samples are separated by a wide compositional gap between ~52 and 68 wt% and often plot along differentiation trends that show different slopes. MgO, $Fe_2O_3^{tot}$, TiO_2, CaO, P_2O_5 and Sr are negatively correlated with SiO_2 suggesting dominantly fractionation of olivine, clinopyroxene and titanomagnetite for the mafic samples. The mafic samples have low contents of Ni (<105 ppm), Cr (<56 ppm) and Co (<40 ppm) supporting the fractionation of olivine ± clinopyroxene. The felsic samples have higher Al_2O_3/CaO ratios than those of the mafic samples. The increase of the Al_2O_3/CaO ratio based on the rise of SiO_2 indicates that amphibole ± plagioclase fractionation is an important process in the felsic rocks. Moreover, the negative correlations for Sr, Zr and P_2O_5 against SiO_2 indicate that plagioclase with accessory zircon and apatite fractionations have affected the felsic samples (Fig. 6). Hasandağı, Erciyes and Acıgöl Quaternary bimodal volcanic rocks closely overlap with the mafic

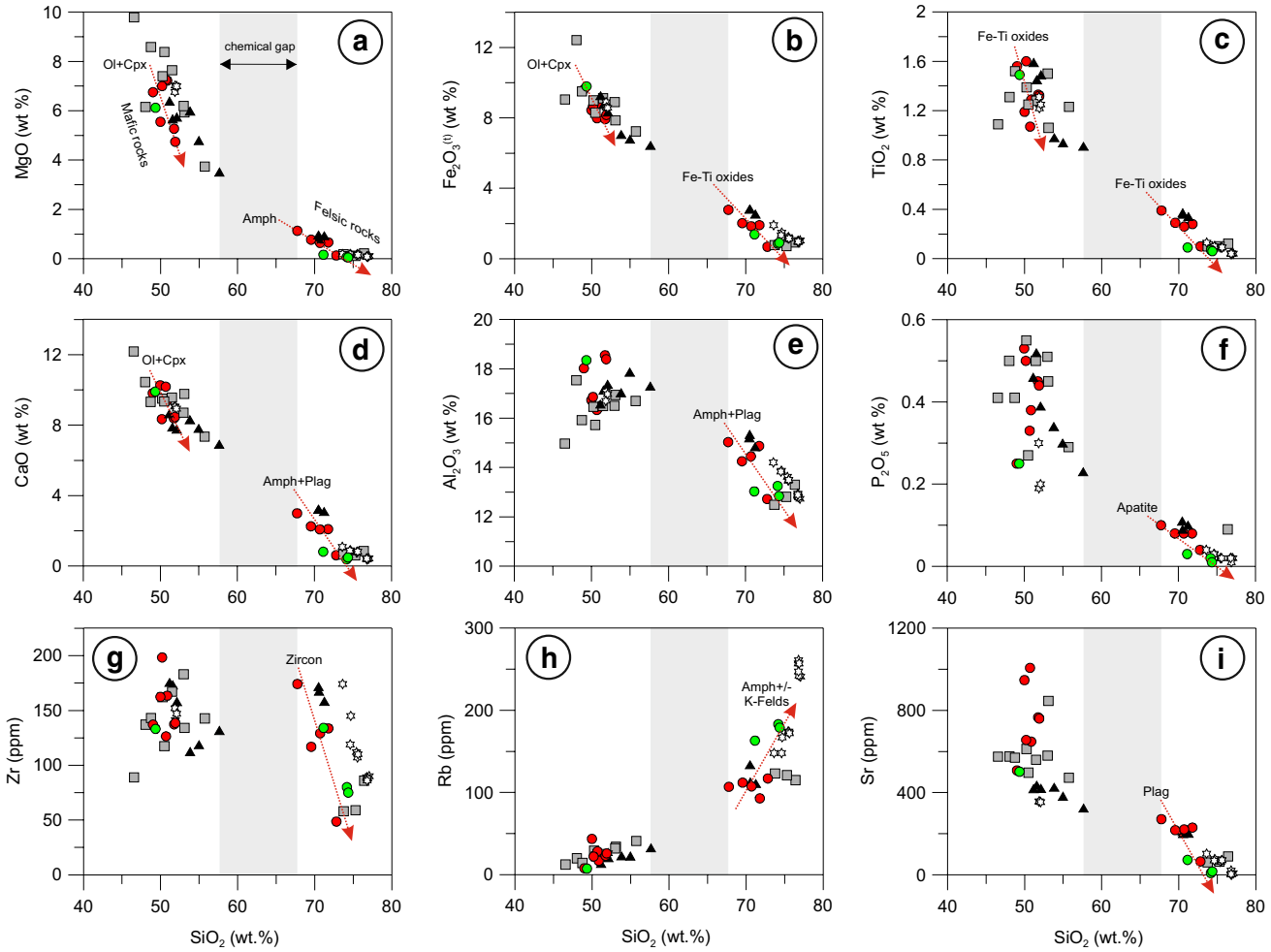

Fig. 6 Selected Harker variation diagrams for the mafic and felsic samples of the NVC. Symbols are the same as in Fig. 5a

samples from Quaternary cinder cones and those of the NVC (Aydar 1997; Deniel et al. 1998; Kürkçüoğlu et al. 1998; Siebel et al. 2011).

The N-MORB normalized trace element patterns of the felsic rocks show strong enrichments of highly incompatible trace elements and slight depletions in less incompatible trace elements that are very similar to average upper continental crust (Fig. 7b). The exceptions are negative Ba, Sr, Eu and Ti anomalies indicative of fractionation of feldspar and Fe–Ti oxides (Fig. 7b). Spikes in two Göllüdağ samples at Hf are enigmatic: They could indicate the presence of a Hf-rich accessory such as zircon or rutile, but zircon would also require excess Zr which is not observed, whereas rutile was not petrographically observed (Fig. 7b). In general, the mafic rocks are enriched relative to N-MORB with trace element patterns that are similar to those of lower continental crust (Fig. 7a). Mafic rocks have concave-upwards REE patterns with $(La/Yb)_N = 4–11$ which is less fractionated than the felsic rocks with $(La/Yb)_N = 9–16$. In addition, REE patterns of the mafic samples do not exhibit any significant negative Eu anomaly (Fig. 7c) while those of the felsic rocks clearly display negative Eu anomalies, supporting extensive plagioclase fractionation during the evolution of the parental magmas (Fig. 7d).

Sr–Nd–Pb whole-rock radiogenic and $\delta^{18}O$ zircon stable isotopes

$^{87}Sr/^{86}Sr$ and $^{143}Nd/^{144}Nd$ isotopic compositions of the studied mafic and felsic rocks generally vary over a narrow range ($^{87}Sr/^{86}Sr = 0.7038–0.7053$; $^{143}Nd/^{144}Nd = 0.5126–0.5128$) and are similar to other bimodal rocks from the CVP (Fig. 8; Table 2). The exceptions are $^{87}Sr/^{86}Sr$ isotopic compositions of Göllüdağ sample Goell-P and Acıgöl felsic rocks which are higher in $^{87}Sr/^{86}Sr$ at the same $^{143}Nd/^{144}Nd$ compared to other samples. A low Sr content makes the samples prone to crustal contamination or addition of extrinsic radiogenic Sr via alteration (Siebel et al. 2011). In case of sample Goell-P which has a Sr content of 72 ppm, the $^{87}Sr/^{86}Sr$ was most likely enhanced by

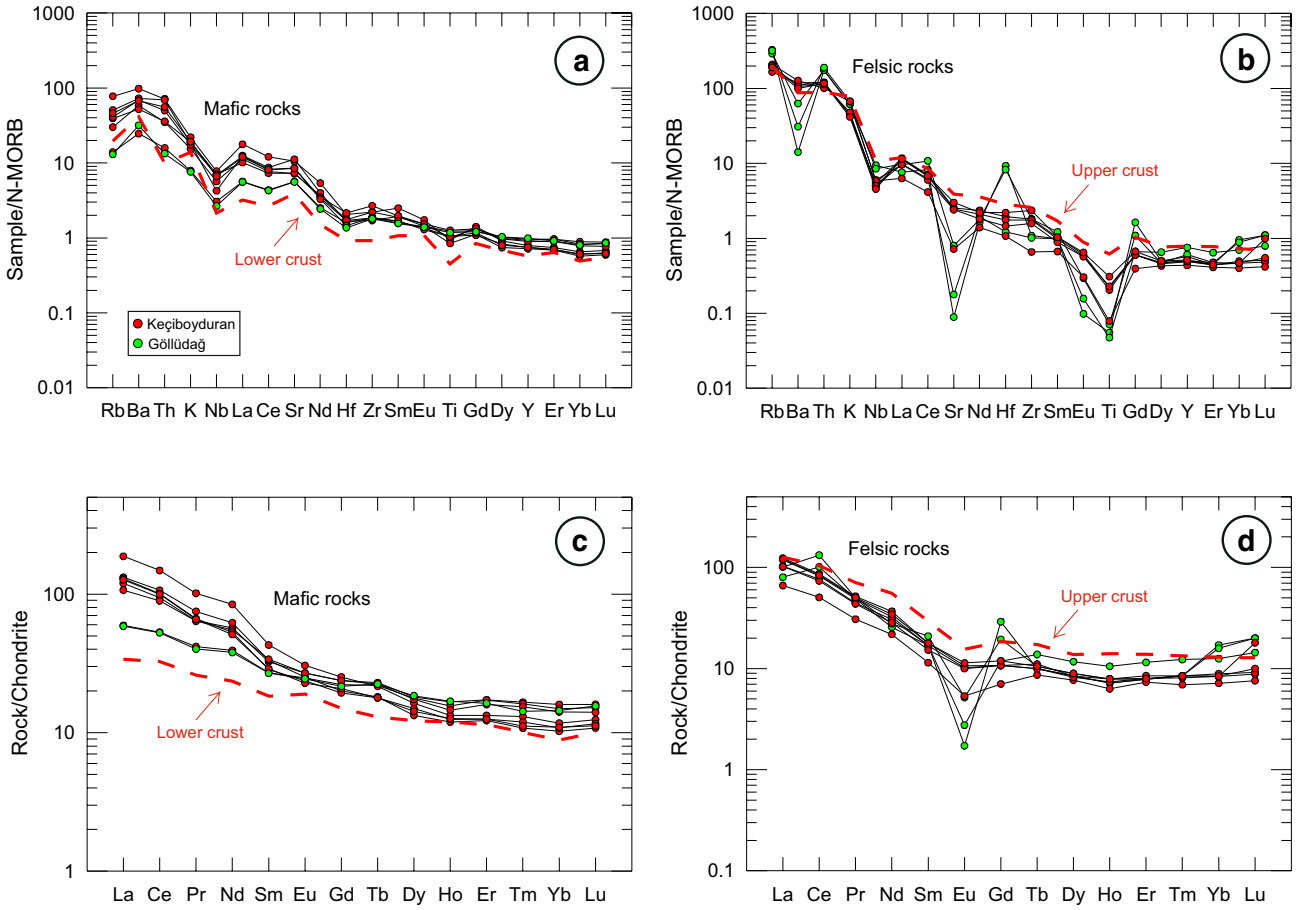

Fig. 7 N-MORB-normalized multi-element variation patterns of **a** mafic and **b** felsic rocks of the NVC. Chondrite-normalized rare earth element abundance patterns of **c** mafic and **d** felsic rocks for the Niğde bimodal series. Values used for normalization are tabulated in Sun and McDonough (1989); lower and upper crust compositions from Rudnick and Gao (2004)

crustal contamination. The most mafic sample of the NVC has $^{87}Sr/^{86}Sr = 0.7038$ and $^{143}Nd/^{144}Nd = 0.5128$, close to the composition of a regional mafic xenolith (Aydin et al. 2011) and other Quaternary alkaline basalts (Güleç 1991) from western Anatolia (Fig. 8). The studied felsic and mafic rocks are homogeneous in Pb isotope composition ($^{206}Pb/^{204}Pb = 18.81–18.92$, $^{207}Pb/^{204}Pb = 15.62–15.68$ and $^{208}Pb/^{204}Pb = 38.80–39.09$) (Figs. 9a and 9b, Online Resource 3), with compositions that are similar to that of EM II.

Zircon has the advantage that it is resistant against alteration and thus better suited to constrain magmatic $\delta^{18}O$ compared to whole-rock or glass analysis. Zircon in NVC felsic rocks have relatively low $\delta^{18}O$ values (average 5.6 ± 0.6 ‰, $n = 40$) closely overlapping mantle values (5.3 ± 0.3 ‰, Fig. 9). The standard deviation is only slightly larger than the analytical reproducibility which suggests a largely homogeneous zircon composition for all samples.

Discussion

Crystallization ages of bimodal volcanism

$^{40}Ar/^{39}Ar$ eruption ages for mafic rocks in the vicinity of Göllüdağ and Keçiboyduran indicate protracted volcanic activity between ~530 and 224 ka (Table 4, Online Resource 2). These ages overlap U–Pb zircon crystallization ages of Keçiboyduran samples (average ages between ~447 and 339 ka), but postdate the eruption age of a basalt (654 ka) which is approximately equidistant between Keçiboyduran and Göllüdağ (Table 3, Online Resource 1). Göllüdağ U–Pb zircon crystallization ages (averages between 889 and 1,083 ka) are distinctly older and suggest a temporal hiatus between volcanism centered around Keçiboyduran and Göllüdağ. At face value, these data indicate younging from northeast (Göllüdağ) to southwest (Keçiboyduran), but the sampling density is insufficient to establish a firm age trend. In any case, our data indicate

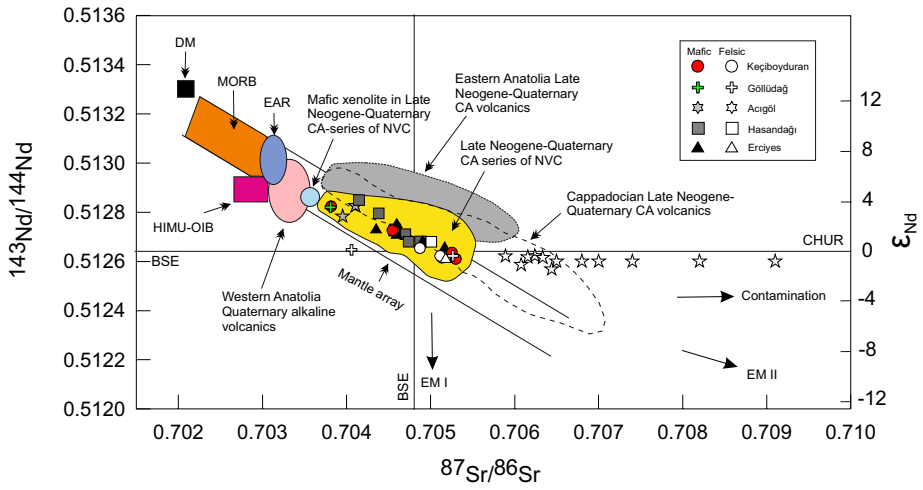

Fig. 8 $^{144}Nd/^{143}Nd$ versus $^{87}Sr/^{86}Sr$ diagram of the bimodal rock series of the NVC. *Data sources* late Neogene–Quaternary calc-alkaline series of the NVC and a xenolith from the NVC, Cappadocian late Neogene–Quaternary calc-alkaline volcanics, Eastern Anatolia Neogene–Quaternary calc-alkaline volcanics and Western Anatolia Quaternary alkaline volcanics taken after Aydin et al. (2011), Deniel et al. (1998), Temel et al. (1998), Pearce et al. (1990) and Güleç (1991), respectively. BSE (Bulk Silicate Earth) composition from Hart et al. (1992). EAR-isotopic composition of shallow asthenosphere (European Asthenospheric Reservoir) beneath Western and Central Europe from Granet et al. (1995). Fields for depleted mantle (DM) and enriched mantle-type HIMU-OIB are from Zindler and Hart (1986)

that mafic and felsic magmatism was broadly coeval. This establishes a potential genetic link between the bimodal end members of the NVC regardless of the distinct ages for each center.

$^{40}Ar/^{39}Ar$ eruption and zircon crystallization ages overlap for the same unit within uncertainty, which suggests comparatively rapid zircon crystallization with brief pre-eruptive zircon residence. This is also supported by the uniformity of zircon ages with only two exceptions where U–Pb zircon ages are older by several 100 ka compared to the dominant age population. Crustal xenocrysts are absent, just as in the Acıgöl rhyolites (Schmitt et al. 2011). The lack of xenocrystic zircon is consistent with rhyolites having similar radiogenic and oxygen isotopic composition to mafic rocks, implying consanguinity between the compositional end members of the NVC bimodal suite.

Petrogenesis of bimodal volcanic rocks

Before discussing the origin and source region characteristics of the bimodal volcanic rocks, the assessment of effects of fractional crystallization combined with the crustal assimilation against magma mixing processes on the composition of the studied rocks are of great importance.

FC and AFC processes versus magma mixing

The mafic samples of the NVC are characterized by low Ni (<105 ppm), Cr (<56 ppm) and Co (<40 ppm) contents. Mg# values (51–62) are high (Table 1) but lower than in primary basalt magmas from the mantle (e.g., Wilson 1989). These geochemical features can be obtained by fractionation of Si-poor mafic phases such as olivine, clinopyroxene and Fe–Ti oxides. Negative correlations of MgO, Fe_2O_3, TiO_2 and CaO contents against SiO_2 (Fig. 6a–e) support this inference because decreases in these element concentrations are expected during fractionation of these minerals. In addition, we observe a positive correlation between $^{87}Sr/^{86}Sr$ and SiO_2 and a negative correlation between $^{143}Nd/^{144}Nd$ and SiO_2; both trends are expected for increasing crustal contamination during differentiation (Fig. 10a, b). Although similar major and trace element and isotopic trends can result from magma mixing/mingling, kinked trends (Fig. 6) and pronounced compositional gaps argue against this and instead favor fractional crystallization and assimilation (AFC). This is supported by the presence of granitic xenoliths in the mafic rocks (Fig. 2h). In contrast to the Harker diagrams (Fig. 6), variation diagrams that use the element versus element ratio (Fig. 10c–e; see also Langmuir et al. 1978) lack a compositional gap and instead display linear trends over the entire compositional range. These diagrams point to a genetic link between the mafic and felsic rocks and to the role of crustal assimilation during the petrogenesis of the NVC bimodal suite.

The felsic rocks of the NVC have wide ranges in major and trace element contents (e.g., $SiO_2 \approx 67$ to 74 wt%) that can be explained by crystal fractionation. The negative correlations of CaO, Al_2O_3, Fe_2O_3, TiO_2, Zr and Sr versus SiO_2 (Fig. 6a–e) indicate the fractionation of amphibole ± plagioclase ± Fe–Ti oxides ± zircon. The pronounced negative

Table 2 Sr-Nd–Pb and $\delta^{18}O$ isotopic compositions of the Niğde bimodal volcanic rocks

Sample No	Sample Group	Rock Type	Age (ka)	Rb (ppm)	Sr (ppm)	$^{87}Rb/^{86}Sr$	$^{87}Sr/^{86}Sr$	I_{Sr} (<1 Ma)	Sm (ppm)	Nd (ppm)	$^{147}Sm/^{144}Nd$	$^{143}Nd/^{144}Nd$	$e_{Nd}(0)$	$f_{Sm/Nd}$	$e_{Nd}(T)$ (<1 Ma)	T_{DM} (Ga)	$^{206}Pb/^{204}Pb$	$^{207}Pb/^{204}Pb$	$^{208}Pb/^{204}Pb$	δO
Goell	Felsic	Ry-lava	1,089	183	8	66.338	0.70500	0.70406	2.60	12.0	0.13099	0.51265	0.2	−0.33	0.2	0.93	18.8720	15.6530	38.9800	5.70
Goell-P	Felsic	Ry-pumice	899	163	72	6.565	0.71350	0.71342	3.20	13.0	0.14881	0.51261	−0.5	−0.24	−0.5	1.27	18.8680	15.6490	38.9660	
G-K2	Felsic	Ry-lava		179	16	32.426	0.70573	0.70527	2.60	14.3	0.10992	0.51262	−0.3	−0.44	−0.3	0.78	18.9110	15.6710	38.9030	5.39
G-C2	Mafic	B-lava		7	502	0.042	0.70381	0.70381	4.10	17.7	0.14004	0.51282	3.6	−0.29	3.7	0.67				
K-51	Mafic	B-lava	654	17	648	0.075	0.70455	0.70455	4.96	26.6	0.11273	0.51273	1.7	−0.43	1.7	0.64	18.8957	15.6739	39.0034	
K-61	Mafic	B-lava		8	508	0.045	0.70382	0.70382	4.15	18.3	0.13710	0.51282	3.6	−0.30	3.6	0.65	18.8080	15.6214	38.7988	
K-75	Mafic	B-scoria		44	947				6.56	39.3										
K-83	Mafic	B-scoria		28	1,007				5.08	29.0										
K-63	Mafic	TB-lava	224	22	656				5.18	25.7										
K-81	Mafic	TB-lava	490	23	766	0.087	0.70526	0.70525	4.36	24.8	0.10629	0.51264	0.0	−0.46	0.0	0.73	18.9128	15.6749	39.0546	
K114	Mafic	TB-lava		26	760	0.098	0.70530	0.70530	4.41	23.9	0.11155	0.51261	−0.5	−0.43	−0.5	0.81	18.9212	15.6856	39.0917	
K-84	Felsic	Ry-lava	447	93	229	1.173	0.70514	0.70514	2.71	17.2	0.09525	0.51262	−0.4	−0.52	−0.4	0.69	18.8486	15.6749	38.9883	5.45
K110	Felsic	Ry-lava	530	107	221				2.58	15.2										
KEC-1	Felsic	Ry-pumice	438	117	65	5.244	0.70491	0.70488	1.75	10.2	0.10372	0.51265	0.3	−0.47	0.3	0.69	18.8547	15.6443	38.9331	6.00
KEC-2	Felsic	Ry-pumice	349	112	217	1.496	0.70513	0.70512	2.34	13.3	0.10637	0.51262	−0.3	−0.46	−0.3	0.75	18.8737	15.6504	38.9642	5.87
K102P	Felsic	Ry-pumice	339	107	270				2.73	16.1										5.52

$e_{Nd} = (((^{143}Nd/^{144}Nd)_s/(^{143}Nd/^{144}Nd)_{CHUR} - 1) \times 10{,}000$, $f_{Sm/Nd} = (^{147}Sm/^{144}Sm)_s/(^{147}Sm/^{144}Sm)_{CHUR} - 1$, $(^{143}Nd/^{144}Nd)_{CHUR} = 0.512{,}638$ and $(^{147}Sm/^{144}Sm)_{CHUR} = 0.1967$. The model ages were calculated using a linear isotopic ratio growth equation: $T_{DM} = 1/l \times \ln(1 + ((^{143}Nd/^{144}Nd)_s - 0.51315)/((^{147}Sm/^{144}Nd)_s - 0.2137))$

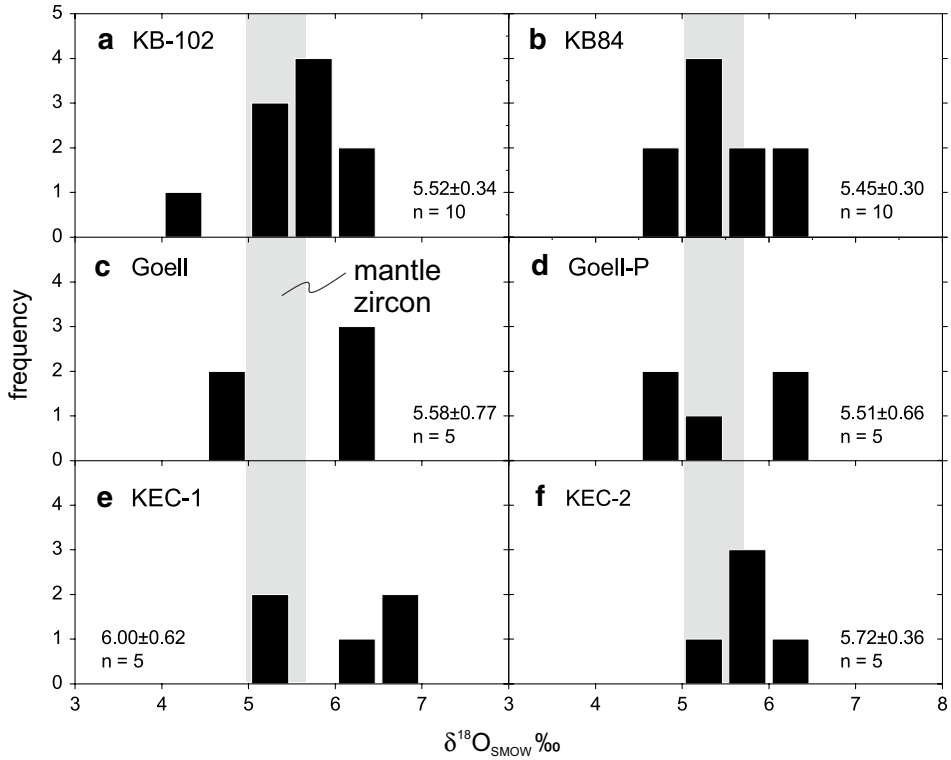

Fig. 9 Histogram of $\delta^{18}O$ (zircon) for felsic samples from the NVC. *Grey columns* indicate average $\delta^{18}O$ of mantle zircons (from Hoefs 2009)

Eu anomalies in the chondrite-normalized REE patterns of the Göllüdağ felsic rocks suggest a significant amount of plagioclase fractionation. Simple fractional crystallization of mafic parental magma to produce the felsic magmas, however, is inconsistent with the lack of intermediate compositions. Instead, it requires some special conditions to explain the wide compositional gap (49–52 to 67–74) in the NVC rock series. Several different controls on the formation of fractionation-generated composition gaps had been proposed. These include (1) a physical control (e.g., Jones 1979), (2) a phase equilibrium control (e.g., Grove and Baker 1984), (3) sidewall crystallization and liquid fractionation (e.g., Chen and Turner 1980; McBirney et al. 1985) and (4) closed-system fractional crystallization (e.g., Thompson 1972). Subsequently, many researchers (Brophy 1991; Francalanci et al. 1995; Pe-Piper and Moulton 2008; Deering et al. 2011; Rooney et al. 2012) suggested that such compositional gaps may develop in magma chambers as a result of the sensitivity of the rheology to crystal contents (i.e., critical crystallinities) and the magmatic silica content which collectively control the relative rates of crystal settling and crystal retention.

Origin and source characteristics of the mafic rocks

The NVC mafic samples are characterized by high concentrations of incompatible trace elements (LILE and LREE) and negative Nb, Hf and Ti anomalies (Fig. 7a), implying that they were not derived from normal MORB- or OIB-like mantle sources, which typically display no or positive Nb–Ti anomalies in N-MORB-normalized trace element diagrams (e.g., Hofmann 1997). On a chondrite-normalized diagram (Fig. 7c), all mafic samples exhibit similar REE element patterns with enrichments in LREE. Furthermore, the contrasting Sr–Nd isotopes between the NVC mafic samples and mafic lower crust preclude the possibility that the samples were produced by partial melting of mafic lower crust. NVC samples have comparatively low Nb/La ratios (0.3–0.7, mostly ≤ 0.5) which is consistent with their derivation from a lithospheric mantle source or a mixed origin involving lithospheric and asthenospheric sources, whereas higher Nb/La (>1) would be required for an OIB-like asthenospheric mantle source (Bradshaw and Smith 1994; Smith et al. 1999). The low Ni (38–103 ppm) content relative to unfractionated mafic magmas (Ni = 200–450 ppm) suggests that the melts underwent significant fractionation of olivine and pyroxene. The Al_2O_3 contents (16.3–18.4 wt%) are higher than those of any mafic parent melts (Al_2O_3 < 15 wt%) in equilibrium with the mantle source. This can be explained by fractionation of some Al-poor mafic phases such as olivine and orthopyroxene. Based on $^{87}Sr/^{86}Sr$ and $^{143}Nd/^{144}Nd$ ratios and enrichments in LILE and LREE, we propose a mantle source that chemically resembled the EM II-type end member. The EM II-type is generally interpreted to represent mantle with recycled terrigeneous sediments from an earlier subduction

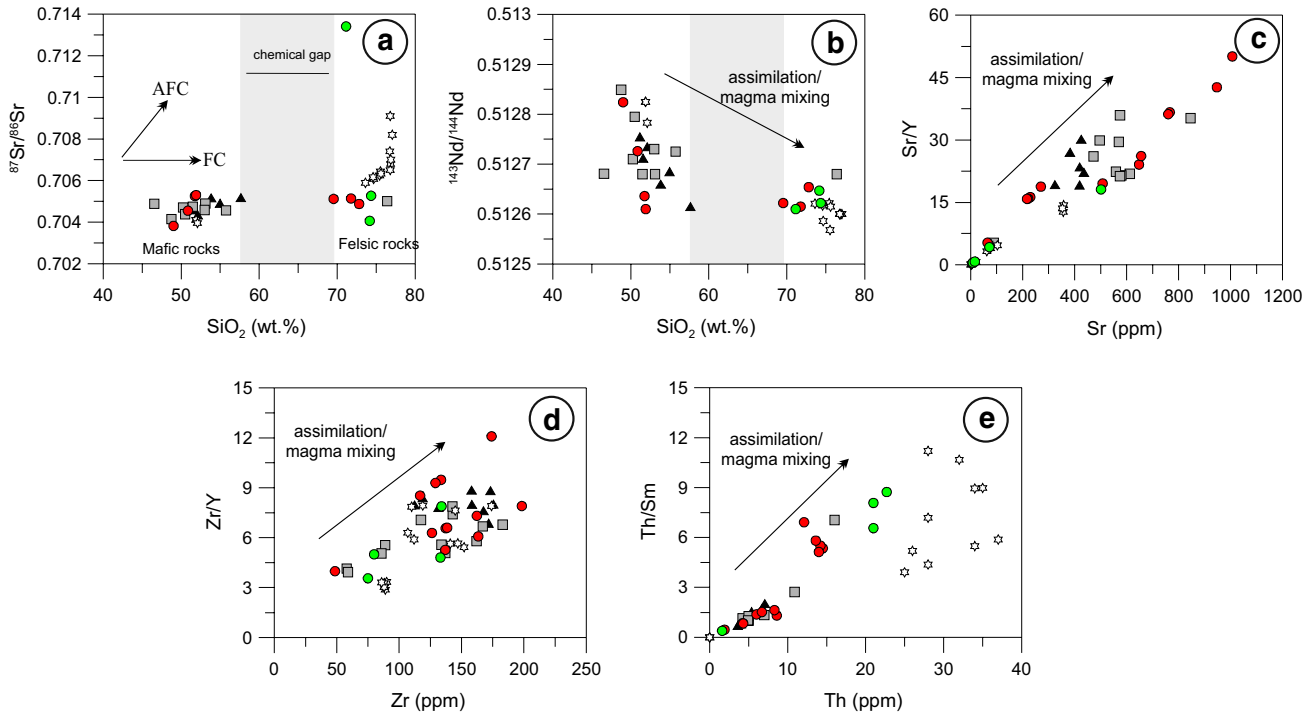

Fig. 10 Geochemical correlation diagrams, depicting the dominant magmatic processes for the bimodal rocks of the NVC. Symbols are the same as in Fig. 5a. **a** $^{87}Sr/^{86}Sr$ versus SiO_2, **b** $^{144}Nd/^{143}Nd$ versus SiO_2, **c** Sr/Y versus Sr, **d** Zr/Y versus Zr and **e** Th/Sm versus Th

event (Zindler and Hart 1986; Beccaluva et al. 2004). This interpretation is also consistent with the Pb isotopic ratios of NVC samples (Figs. 9a and 9b, Online Resource 3).

Enrichments in LILE and LREE with negative Nb–Ti anomalies are characteristics of subduction-related magmas and are commonly attributed to an originally depleted mantle source, which has been previously enriched in LILEs over HFSE by fluids or sediments derived from the subducted slab (e.g., Pearce 1982; Hawkesworth et al. 1997; Elburg et al. 2002; Aydin et al. 2008). An important feature during subduction-related mantle metasomatism is the formation of hydrous mineral phases such as phologopite and/or amphibole (e.g., Beccaluva et al. 2004). Comparison between elements with different compatibilities in phlogopite and amphibole can help to identify the presence of these minerals in the mantle source (Furman and Graham 1999; Yang et al. 2004). Considering the most primitive NVC sample K-51, its Ba/Rb (21.8) and Nb/Th (3.1) ratios are relatively high, whereas Rb/Sr (0.03) is low, suggesting that the source region contained amphibole rather than phlogopite.

Spinel is depleted in REE and Y, whereas garnet is enriched in HREE and Y, and amphibole is enriched in MREE. Residual garnet during melting will result in HREE depletions, with Y/Yb > 10 and $(Ho/Yb)_N$ values > 1.2 (e.g., Ge et al. 2002). Sample K-51 is depleted in HREE, with Y/Yb = 9.9 and $(Ho/Yb)_N$ = 1.02, implying that melting occurred at depths above the garnet stability field where spinel and/or amphibole were present in the residue. The quasi-flat HREE patterns (Fig. 7c) support this inference. The lack of any significant MREE enrichment in the mafic samples (Fig. 7c) suggests that amphibole was present in the residue after partial melting. Therefore, we infer that the NVC mafic source was an amphibole-bearing spinel peridotite. This is in accordance with the isotopically depleted characteristics of the NVC mafic rocks ($^{87}Sr/^{86}Sr$ = 0.70381–0.70530, $^{143}Nd/^{144}Nd$ = 0.51261–0.51283 with εNd from −0.5 to 3.6; Table 2).

Origin of the felsic rocks and petrologic modeling

Thorium is used as a proxy of differentiation from mafic (basaltic) to felsic (rhyolitic) rocks in the fractional crystallization and assimilation processes because of the strong positive correlation with SiO_2 in bimodal NVC rocks. NVC mafic rocks show a positive correlation between $^{87}Sr/^{86}Sr$ and Th (Fig. 11) consisting with AFC involving continental crust. By contrast, NVC rhyolites are characterized by a slightly negative correlation between $^{87}Sr/^{86}Sr$ and Th if sample G-K2 is excluded (Fig. 11). Invariant or decreasing $^{87}Sr/^{86}Sr$ with increasing Th implies that the rhyolite magmas evolved via pure FC or were contaminated by wall rocks having lower $^{87}Sr/^{86}Sr$ than the basaltic parent magmas.

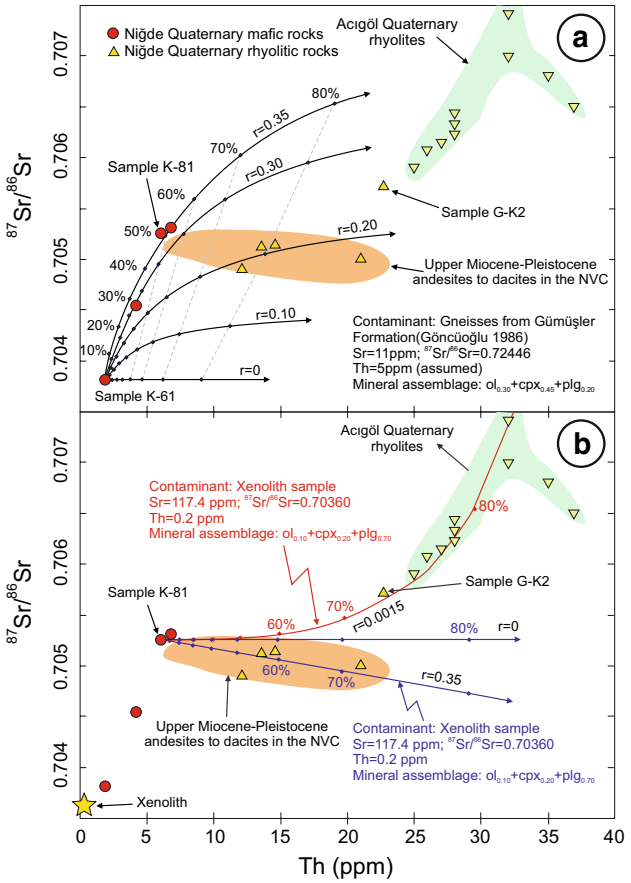

Fig. 11 AFC modeling of the Quaternary bimodal volcanic rocks from the NVC. **a** $^{87}Sr/^{86}Sr$ versus Th diagram for mafic samples and **b** $^{87}Sr/^{86}Sr$ versus Th diagram for felsic samples

Gneissic rocks from the Gümüşler Formation of the Niğde Massif (Göncüoğlu 1986) are characterized by highly radiogenic Sr ratios ($^{87}Sr/^{86}Sr$ up to 0.72464) and are used as a potential contaminant in AFC modeling for the basaltic rocks. Sample K-61, which has the lowest $^{87}Sr/^{86}Sr$ ratio and Th content, is used as starting composition for AFC models (Fig. 11a). In the light of the petrographic observations, the fractionating mineral assemblage is fixed at $Ol_{0.30} + Cpx_{0.45} + Plg_{0.20}$ for the studied mafic rocks. The AFC modeling results show that the geochemical features of the basaltic and basaltic-andesitic rocks require assimilation of gneissic rocks with $r \approx 0.35$ (r = ratio of assimilated over crystallized material) and $F \approx 50$ % (F = fraction of melt remaining).

Samples from Quaternary NVC rhyolites together with those from late Miocene–Pliocene NVC andesites to dacites show a slightly negative correlation on the $^{87}Sr/^{86}Sr$ versus Th diagram (Fig. 11). This may indicate that both rock suites either evolved via closed-system fractional crystallization or were contaminated by crustal rocks with lower radiogenic Sr contents. Moreover, the comparatively high Th coupled with low $^{87}Sr/^{86}Sr$ (relative to the parental composition K-81) of all samples except G-K2 rules out the gneissic rocks from the Gümüşler Formation as the sole contaminant. In this context, it is also noteworthy that sample G-K2 is geochemically intermediate between the Quaternary NVC rhyolites and the Acıgöl rhyolites in the region (see Fig. 11b). Integrating these observations, a closed-system FC and two AFC models are constructed and presented in Fig. 11b. An AFC evolution of the evolved starting magma composition K-81 involving a crustal contaminant represented by a xenolith sample with comparatively low $^{87}Sr/^{86}Sr$ may explain the geochemical features of most NVC rhyolitic rocks ($r = 0.35$), except for anomalous sample G-K2 (Fig. 11b). To explain the composition of sample G-K2, a second AFC model is required involving the crustal contaminant with elevated $^{87}Sr/^{86}Sr$ typical for regional gneissic rocks at low r value ($r = 0.0015$). This model can also explain the high $^{87}Sr/^{86}Sr$ of the Quaternary Acıgöl rhyolites. Overall, the data show that the rhyolitic rocks can be modeled starting from an evolved mafic rock sample by ~70–75 % fractionation of an assemblage of $Ol_{0.10} + Cpx_{0.20} + Plg_{0.70}$ and an additional, low-degree contamination from distinct crustal wall rocks.

Geodynamic scenario for the Quaternary bimodal volcanism

The late Mesozoic to early Cenozoic geology of the eastern Mediterranean region was controlled by multiple collisional events between the Afro-Arabian plates in the south and the Anatolide-Tauride block and Eurasian platform in the north, which resulted in N–S shortening across much of Anatolia (Şengör et al. 1985; Dewey et al. 1986; Bozkurt 2001; Dilek 2006). After the collisions, the Anatolide-Tauride block was trapped between major continental blocks and subjected to crustal thickening and uplift. Subsequent extensional collapse during the early-middle Cenozoic (Whitney and Dilek 1997, 1998) produced several Cordilleran-type metamorphic core complexes including the Niğde Massif in the study area. During this stage, the central Anatolian basement was intruded by granitic and gabbroic rocks (Kadıoğlu et al. 2003; Ilbeyli et al. 2004; Köksal et al. 2004; Boztuğ et al. 2007). Post-collisional extensional tectonics also played a major role in the evolution of the central Anatolia and the development of its landscape from late Cenozoic to Recent (Dilek 2006; Dilek and Whitney 2000). Further lithospheric thinning related to lateral crustal escape along major strike-slip faults and tectonic subsidence coincided with the formation of extensive young volcanic provinces in Turkey including the Cappadocia region in central Anatolia (Şengör et al. 1985; Dilek and Whitney 2000; Tatar et al. 2002).

The CVP is characterized by late Neogene to Quaternary stratovolcanoes and widespread volcaniclastic deposits with a calc-alkaline character and Quaternary felsic domes and cinder cones or scoria deposits with related mafic lavas that display bimodal chemistry with basaltic or basaltic andesitic and rhyolitic compositions (Göncüoğlu and Toprak 1992; Toprak 1998; Aydin 2008; Siebel et al. 2011). These volcanic edifices commonly form linear clusters along and/or at the intersections of the Tuzgölü (TF) and Ecemiş fault (EF) systems, suggesting interaction between faulting and volcanism (Toprak and Göncüoğlu 1993; Dirik and Göncüoğlu 1996). Pliocene–Quaternary volcanic and volcaniclastic rocks of major stratovolcanoes such as Erciyes, Hasandağı and Melendiz are crosscut by these fault systems and in turn overlie segments of the faults, indicating that faulting and volcanism was largely contemporaneous (Dirik and Göncüoğlu 1996; Toprak 1998). These relations suggest that magma transport and extrusions of lavas and volcaniclastic rocks were facilitated by transtensional strike-slip fault systems (Dilek and Whitney 2000; Dirik 2001).

Late Neogene–Quaternary volcanism of the CVP is generally hypothesized to be fueled by active subduction along the Cyprean arc (Innocenti et al. 1975; Temel et al. 1998) or by paleo-subduction of this arc with major volcanic centers in the region interpreted as remnants of this arc (e.g., Reilinger et al. 1997). The geochemical characteristics of the Cappadocian volcanic rocks, however, indicate pronounced changes from calc-alkaline to Na-alkaline through time (Miocene–Pliocene to Pleistocene) and thus do not support a pure subduction origin. Recent studies have suggested the contribution of an asthenospheric mantle source with a subduction-related geochemical signature (Aydin 2008; Gençalioğlu-Kuşçu and Geneli 2010; Aydin et al. 2011). Crustal-scale seismic tomography has imaged the subducted portion of the African lithosphere between the Cyprus trench and southwestern Anatolia (Gans et al. 2009; Dilek and Sandvol 2009; Dilek and Altunkaynak 2009) with the seismic anomaly being located east of Cyprus (Piromallo and Morelli 2003; Faccenna et al. 2006). In particular, some studies have pointed out that subduction along the Cyprus section of the trench is impeded by the collision of the Eratosthenes Seamount, which is a part of the African promontory (Robertson and Grasso 1995; Glover and Robertson 1998). On tomographic images of Biryol et al. (2011), the region defined as the CVP is directly underlain by slow velocity perturbations on the order of 1–2 % that extend as deep as 200 km. It is possible that these slow anomalies are due to the presence of ascending, hot, buoyant asthenosphere containing partial melts, which are responsible for the CVP volcanism. Although the current outline of the Cyprus slab and the seismic anomalies favor a dominantly asthenospheric mantle source for the latest phase of volcanism in the region, in accord with results of Aydin (2008) and Aydin et al. (2012), a contribution from the subduction of the Cyprus slab cannot be ruled out based on its close proximity to the ascending asthenosphere. Hence, this configuration might explain the special characteristics of mafic volcanism (calc-alkaline to Na-alkaline) observed in the CVP including the NVC (Aydin 2008; Gençalioğlu-Kuşçu and Geneli 2010; Aydin et al. 2011; Siebel et al. 2011). Additionally, the geochronological and geochemical data suggest that felsic and mafic rocks of the NVC are genetically closely related to each other. Hence, mantle-derived differentiated basaltic melts which experienced fractional crystallization and low degree of crustal assimilation are suggested to be the parent melt of the felsic volcanics.

Conclusions

From U–Pb and ^{40}Ar-^{39}Ar dating, whole-rock geochemistry, Sr–Nd–Pb radiogenic and δ^{18}O stable isotope studies on Quaternary bimodal volcanic rocks of the Niğde Volcanic Complex (NVC), Cappadocia province of central Anatolia, we arrive at the following conclusions:

New geochronological data suggest that Pleistocene bimodal volcanic activity in the NVC occurred between ca. 1.1 and ca. 0.2 Ma. Mafic rocks associated with cinder cones in the NVC formed between 654 and 224 ka, while the latest felsic products of Göllüdağ and around Keçiboyduran formed between ca. 1,080–900 ka and ca. 450–340 ka, respectively.

A distinct compositional gap is evident between (1) mafic volcanics consisting of basalts, trachybasalts, basaltic andesites and scoria lapilli fall-out deposits with mainly basaltic composition and (2) felsic volcanics consisting of mostly rhyolitic lavas and pumice lapilli fall-out and surge deposits with dacitic to rhyolitic composition.

Ne-normative Pleistocene mafic volcanic rocks have isotopic characteristics similar to Miocene–Pliocene calc-alkaline volcanic rocks in the region; their parental magmas originated from a mixed origin of isotopically depleted and chemically enriched lithospheric mantle material (amphibole-bearing spinel peridotite), which was metasomatized by previous slab-derived fluids, with a lesser amount of asthenospheric mantle.

The geochemical characteristics of the bimodal volcanic rocks indicate multi-stages of FC and/or AFC processes. AFC modeling suggests that the mafic rocks were contaminated by high ^{87}Sr/^{86}Sr wall rocks. Felsic samples lack evidence for further crustal contamination unless this involved wall rocks with low ^{87}Sr/^{86}Sr and were derived from basaltic parental melts via fractional crystallization.

Geochronological and geochemical results combined with regional geological and geophysical data suggest that the Cappadocian volcanism changed from calc-alkaline to Na-alkaline through time (late Neogene to Quaternary); younger Ne-normative mafic rocks do not reflect a pure subduction origin. These data also provide convincing evidence that bimodal activity in the NVC and the CVP, in general, developed in a post-collisional extensional tectonic regime, which played a key role during magma genesis.

Acknowledgments This work was partly supported by the Scientific and Technological Research Council of Turkey (TUBITAK, Grant 108Y003) and the German Science Foundation (Grant Si 718/9-1). The ion microprobe facility at the University of California, Los Angeles, is partly supported by a grant from the Instrumentation and Facilities Program, Division of Earth Sciences, National Science Foundation. The authors are grateful to John Huard for help during Ar–Ar dating and the Niğde University for contributions during the sample preparation processes. The authors sincerely thank Jochen Hoefs for editorial handling and to Oliver Bachman and one anonymous referee for their valuable suggestions, which greatly improved the manuscript.

References

Alıcı Şen P, Temel T, Gourgaud A (2004) Petrogenetic modelling of Quaternary post-collisional volcanism: a case study of central and eastern Anatolia. Geol Mag 141:81–98

Aydar E (1997) Volcanological and petrological characteristics of Karataş volcanites, Central Anatolia. Hacettepe Üniv Yerbilim Derg 19:41–55 (in Turkish with English abstract)

Aydar E, Gourgaud A (1998) The geology of Mount Hasan stratovolcano, central Anatolia, Turkey. J Volcanol Geothermal Res 85:129–152

Aydar E, Gourgaud A, Deniel C, Lyberis N, Gündoğdu N (1995) Le volcanisme quaternaire d'Anatolie centrale (Turquie): association de magmatismes calco-alcalin et alcalin en domaine de convergene. Can J Earth Sci 32:1058–1069

Aydar E, Schmitt AK, Çubukçu HE, Akın L, Ersoy O, Şen E, Duncan RA, Atıcı G (2012) Correlation of ignimbrites in the central Anatolian volcanic province using zircon and plagioclase ages and zircon compositions. J Volcanol Geothermal Res 213–214:83–97

Aydin F (2008) Contrasting complexities in the evolution of calc-alkaline and alkaline melts of the Niğde volcanic rocks, Turkey: textural, mineral chemical and geochemical evidence. Eur J Min 20:101–118

Aydin F, Karsli O, Chen B (2008) Petrogenesis of the Neogene alkaline volcanics with implications for post-collisional lithospheric thinning of the Eastern Pontides, NE Turkey. Lithos 104:249–266

Aydin F, Sönmez M, Dirik K (2011) Geochronology and petrogenesis of Niğde Volcanic Complex: implications on source composition, melt evolution and geodynamic processes in the central anatolia during neo-quaternary. İn: TUBITAK project (grant 108Y003), (Unpublished data)

Aydin F, Siebel W, Uysal I, Ersoy EY, Schmitt A, Sönmez M, Duncan R (2012) Geochemical, isotopic (Sr–Nd–Pb) and geochronological (Ar–Ar and U–Pb) constraints on quaternary bimodal volcanism of the Niğde Volcanic Complex (Central Anatolia, Turkey). In: EGU conference, geophysical research abstracts, vol 14, pp 14300–14302

Bachmann O, Oberli F, Dungan MA, Meier M, Mundil R, Fischer H (2007) $^{40}Ar/^{39}Ar$ and U–Pb dating of the Fish Canyon magmatic system, San Juan Volcanic field, Colorado: evidence for an extended crystallization history. Chem Geol 236:134–166

Batum I (1978) Geochemistry and petrology of Acıgöl and Göllüdağ volcanics at southwest of Nevşehir Central Anatolia, Turkey. Yerbilimleri 4(1–2):70–88 (in Turkish with English abstract)

Beccaluva L, Bianchini G, Bonadiman C, Siena F, Vaccaro C (2004) Coexisting anorogenic and subduction-related metasomatism in the mantle xenoliths from the Betic Cordillera (southern Spain). Lithos 75:67–87

Beekman PH (1966) The Pliocene and quaternary volcanism in the Hasan Dag-Melendiz Dag region. Bull Mineral Res Explor Inst 66:90–105

Besang C, Eckhardt FJ, Harre W, Kreuzer H, Müller P (1977) Radiometrische Altersbestimmungen an neogenen Eruptivgesteinen der Türkei. Geol Jb B25:3–36

Bigazzi G, Yeğingil Z, Ercan T, Oddone M, Özdoğan M (1993) Fission track dating obsidians of central and northern Anatolia. Bull Volcanol 55:588–595

Biryol CB, Beck SL, Zandt G, Özacar AA (2011) Segmented African lithosphere beneath the Anatolian region inferred from teleseismic P-wave tomography. Geophys J Int 184:1037–1057

Bonin B (2004) Do coeval mafic and felsic magmas in post-collisional to within plate regimes necessarily imply two contrasting, mantle and crustal, sources? A review. Lithos 78:1–24

Bozkurt E (2001) Neotectonics of Turkey—a synthesis. Geodin Acta 14:3–30

Boztuğ D, Arehart GB, Platevoet B, Harlavan Y, Bonin B (2007) High-K calc alkaline I-type granitoids from the composite Yozgat batholith generated in a postcollisional setting following continent-oceanic island arc collision in central Anatolia, Turkey. Miner Petrol 91:191–223

Bradshaw TK, Smith EI (1994) Polygenetic Quaternary volcanism at Crater Flat, Nevada. J Volcanol Geotherm Res 63:165–182

Brophy JG (1991) Composition gaps, critical crystallinity, and fractional crystallization in orogenic (calc-alkaline) magmatic systems. Contrib Mineral Petrol 109:173–182

Brown SJA, Fletcher IR (1999) SHRIMP U–Pb dating of the preeruption growth history of zircons from the 340 ka Whakamaru Ignimbrite, New Zealand: evidence for > 250 k.y. magma residence times. Geology 27(11):1035–1038

Chen CF, Turner JS (1980) Crystallization in a double-diffusive system. J Geophys Res 85(2573):2593

Coulon C, Maluski H, Bollinger C, Wang S (1986) Mesozoic and Cenozoic volcanic rocks from central and southern Tibet: $^{39}Ar/^{40}Ar$ dating, petrological characteristics and geodynamic significance. Earth Planet Sci Lett 79:281–302

Coward MP, Dewey JF, Hancock PL (1987) Continental extensional tectonics. Geol Soc Spec Publ 28:1–637

Deering CD, Bachmann O, Dufek J, Gravley DM (2011) Rift-Related transition from andesite to rhyolite volcanism in the Taupo Volcanic Zone (New Zealand) controlled by crystal-melt dynamics in mush zones with variable mineral assemblages. J Petrol 52(11):2243–2263

Deniel C, Aydar E, Gourgaud A (1998) The Hasan Dagi stratovolcano (Central Anatolia, Turkey): evolution from calc-alkaline to alkaline magmatism in a collision zone. J Volcanol Geotherm Res 87:275–302

Dewey JF, Hempton MR, Kidd WSF, Şaroğlu F, Şengör AMC (1986) Shortening of continental lithosphere: the neotectonics of Eastern Anatolia-a young collision zone. In Coward MP, Ries AC (eds) Collision zone tectonics: Geol Soc London Spec Publ 19:3–36

Dilek Y (2006) Collision tectonics of the Eastern Mediterranean region: causes and consequences. Geol Soc Am Spec Paper 409:1–13

Dilek Y, Altunkaynak S (2009) Geochemical and temporal evolution of Cenozoic magmatism in western Turkey: mantle response to collision, slab breakoff, and lithospheric tearing in an orogenic belt. In van Hinsbergen DJJ, Edwards MA, Govers R (eds) Collision and collapse at the Africa–Arabia–Eurasia subduction zone. Geol Soc London Spec Publ 311:213–233

Dilek Y, Sandvol E (2009) Seismic structure, crustal architecture and tectonic evolution of the Anatolian–African Plate Boundary and the Cenozoic orogenic belts in the Eastern Mediterranean region. J Geol Soc London Spec Publ 327:127–160

Dilek Y, Whitney DL (2000) Cenozoic crustal evolution in central Anatolia: extension, magmatism and landscape development: proceedings of the third international conference on the geology of the eastern mediterranean. In: Geological survey department, Nicosia, Cyprus, pp 183–192

Dirik (2001) Neotectonic evolution of the northwestward arched segment of the Central Anatolian Fault Zone, Central Anatolia-Turkey. Geodin Acta 14:147–158

Dirik K, Göncüoğlu C (1996) Neotectonic characteristics of central Anatolia. Inter Geol Rev 38:807–817

Doe BR, Leeman WP, Christiansen RL, Hedge CE (1982) Lead and strontium isotopes and related trace elements as genetic tracers in the upper Cenozoic rhyolite-basalt association of the Yellowstone Plateau volcanic Field. J Geophys Res 87:4785–4806

Druitt TH, Brenchley PJ, Gökten YE, Francaviglia V (1995) Late-Quaternary rhyolitic eruptions from the Acıgöl Complex, central Turkey. J Geol Soc (London) 152:655–667

Duncan AR, Erlank AJ, Marsh J (1984) Regional geochemistry of the Karoo igneous province. Spec Publ Geol Soc Africa 13:355–388

Elburg MA, Bergen MV, Hoogewerff J, Foden J, Vroon P, Zulkarnain I, Nasution A (2002) Geochemical trends across an arc-continent collision zone: magma sources and slab-wedge transfer processes below the Pantar Strait volcanoes, Indonesia. Geochim Cosmochim Acta 66:2771–2789

Ercan T, Tokel S, Matsuda JI, Ul T, Notsu K, Fujitani T (1992) New geochemical, isotopic and radiometric data of the Quaternary volcanism of Hasandağı-Karacadağ (Central Anatolia). TJK Bülteni 7:8–21 (In Turkish with English abstract)

Faccenna C, Bellier O, Martinod J, Piromallo C, Regard V (2006) Slab detachment beneath eastern Anatolia: a possible cause for the formation of the North Anatolian fault. Earth Planet Sci Lett 242:85–97

Francalanci L, Varekamp JC, Vougioukalakis G, Defant MJ, Innocenti F, Manetti P (1995) Crystal retention, fractionation and crustal assimilation in a convecting magma chamber, Nisyros Volcano, Greece. Bull Volcanol 56(8):601–620

Frost CD, Frost BR, Chamberlain KR, Edwards BR (1999) Petrogenesis of the 1.43 Ga Sherman batholith, SE Wyoming, USA: a reduced, rapakivi-type anorogenic granite. J Petrol 40:1771–1802

Frost CD, Bell JM, Frost BR, Chamberlain KR (2001) Crustal growth by magmatic underplating: isotopic evidence from the northern Sherman batholith. Geology 29:515–518

Furman T, Graham D (1999) Erosion of lithospheric mantle beneath the East African Rift system: geochemical evidence from the Kivu volcanic province. Lithos 48:237–262

Gans CR, Beck SL, Zandt G, Biryol CB, Özacar AA (2009) Detecting the limit of slab break-off in Central Turkey: new high-resolution Pn tomography results. Geophys J Int 179:1566–1572

Garland FE, Hawkesworth CJ, Mantovani MSM (1995) Description and petrogenesis of Parana rhyolites, Southern Brazil. J Petrol 36:1193–1227

Ge XY, Li XH, Chen ZG, Li W (2002) Geochemistry and petrogenesis of Jurassic high Sr/low Y granitoids in the eastern China: constraints on crustal thickness. Chin Sci Bull 47:962–968

Geist D, Howard KA, Larson P (1995) The generation of oceanic rhyolites by crystal fractionation: the basalt–rhyolite association at Volcán Alcedo, Galápagos Archipelago. J Petrol 36:965–982

Gençalioğlu Kuşçu G, Geneli F (2010) Review of post- collisional volcanism in the Central Anatolian Volcanic province (Turkey), with special reference to the Tepekoy Volcanic complex. Int Earth Sci (Geol Rdsch) 99:593–621

Gertisser R, Keller J (2000) From basalt to dacite: origin and evolution of the calc-alkaline series of Salina, Aeolian Arc. Italy. Contrib Mineral Petrol 139(5):607–626

Glover C, Robertson AHF (1998) Role of extensional processes and uplift in the Plio-Quaternary sedimentary and tectonic evolution of the Aksu Basin, southwest Turkey. J Geol Soc London 155:365–368

Göncüoğlu MC (1986) Geochronological data from the southern part (Niğde area) of the Central Anatolian Massif. Bull Mineral Res Explor Inst (MTA) 105(106):83–96

Göncüoğlu MC, Toprak V (1992) Neogene and Quaternary volcanism of central Anatolia: a volcano-structural evaluation. Bull de la Section Volcanol Soc Géol France 26:1–6

Granet M, Wilson M, Achauer U (1995) Imaging a mantle plume beneath the Fernando de Noronha. Earth Planet Sci Lett 136:281–296

Grove TL, Baker MB (1984) Phase equilibrium controls on the tholeiitic versus calc-alkaline differentiation trends. J Geophys Res 89:3252–3274

Güleç N (1991) Crust-mantle interaction in Western Turkey: implications from Sr and Nd isotope geochemistry of Tertiary and Quaternary volcanics. Geol Mag 128(5):417–435

Hart S, Hauri EH, Oschmann LA, Whitehead JA (1992) Mantle plumes and entrainment. Science 256:517–520

Hawkesworth CJ, Turner SP, McDermott F, Peate DW, van Calsteren P (1997) U–Th isotopes in arc magmas: implications for element transfer from the subducted crust. Sciences 276:551–555

Hildreth W, Halliday AN, Christiansen RL (1991) Isotopic and chemical evidence concerning the genesis and contamination of basaltic and rhyolitic magma beneath the Yellowstone plateau volcanic field. J Petrol 32:63–138

Hoefs J (2009) Stable isotope geochemistry. Springer, Berlin

Hofmann AW (1997) Mantle geochemistry: the message from oceanic volcanism. Nature 385:219–229

Ilbeyli N, Pearce JA, Thirlwall MF, Mitchell JG (2004) Petrogenesis of collision-related plutonic in Central Anatolia, Turkey. Lithos 72:163–182

Innocenti F, Mazzuoli G, Pasquare F, Radicati Di Brozola F, Villari L (1975) The Neogene calcalkaline volcanism of Central Anatolia: geochronological data on Kayseri-Niğde area. Geol Mag 112(4):349–360

Jones WB (1979) Mixed benmoreite/trachyte flows from Kenya and their bearing on the Daly gap. Geol Mag 116:487–489

Kadıoğlu YK, Dilek Y, Güleç N, Foland KA (2003) Tectonomagmatic evolution of bimodal plutons in the Central Anatolian Crystalline Complex, Turkey. J Geol 111:671–690

Kocyiğit A, Beyhan A (1998) A new intracontinental transcurrent structure: the Central Anatolian Fault Zone, Turkey. Tectonophysics 284:317–336

Köksal S, Göncüoğlu MC (2008) Sr and Nd isotopic characteristics of some S-, I-and A-type granitoids from Central Anatolia. Turk J Earth Sci 17:111–127

Köksal S, Romer RL, Göncüoğlu MC, Toksoy-Köksal F (2004) Timing of post collision H-type to A-type granitic magmatism: U–Pb titanite ages from the Alpine central Anatolian granitoids Turkey. Int J Earth Sci 93:974–989

Koppers AAP (2002) ArArCALC—software for $^{40}Ar/^{39}Ar$ age calculations. Comput Geosci 28(5):605–619

Kürkçüoğlu B, Şen E, Aydar E, Gourgaud A, Gündoğdu N (1998) Geochemical apporoach to magmatic evolution of Mt. Erciyes stratovolcano Central Anatolia, Turkey. J Volcanol Geotherm Res 85:473–494

Lacasse C, Sigurdsson H, Carey SN, Jóhannesson H, Thomas LE, Rogers NW (2007) Bimodal volcanism at the Katla subglacial caldera, Iceland: insight into the geochemistry and petrogenesis of rhyolitic magmas. Bull Volcanol 69:373–399

Langmuir CH, Vocke RD, Hanson GN, Hart SR (1978) A general mixing equation with applications to icelandic basalts. Earth Planet Sci Lett 37:380–392

Le Maitre RW (ed) (2002) A classification of igneous rocks and glossary of terms. In: Recommendations of the international union of geological sciences subcommission on the systematics of igneous rocks. Cambridge University Press, Cambridge

Le Pennec J-L, Bourdier J-L, Temel A, Camus G, Gourgaud A (1994) Neogene ignimbrites of the Nevşehir plateau (central Turkey): stratigraphy, distribution and sources constraints. J Volcanol Geotherm Res 63:59–87

Liu Y, Hu Z, Zong K, Gao C, Gao S, Xu J, Chen H (2010) Reappraisement and refinement of zircon U–Pb isotope and trace element analyses by LA-ICP-MS. Chin Sci Bull 55(15):1535–1546

McBirney AR, Baker BH, Nilson RH (1985) Liquid fractionation. Part I: basic principles and experimental simulations. J Volcanol Geotherm Res 24:1–24

McCulloch MT, Kyser TK, Woodhead JD, Kinsley L (1994) Pb-Sr-Nd-O isotopic constraints on the origin of rhyolites from the Taupo Volcanic Zone of New Zealand: evidence for assimilation followed by fractionation from basalt. Contrib Mineral Petrol 115:303–312

McCurry M, Rodgers DW (2009) Mass transfer along the Yellowstone hotspot track I: petrologic constraints on the volume of mantle-derived magma. J Volcanol Geotherm Res 188(1–3):86–98

McKenzie DP (1972) Active tectonics of the Mediterranean. Geophys J R Astron Soc 30:109–185

Min KW, Mundil R, Renne PR, Ludwig KR (2000) A test for systematic errors in $^{40}Ar/^{39}Ar$ geochronology through comparison with U/Pb analysis of a 1.1-Ga rhyolite. Geochim Cosmochim Acta 64(1):73–98

Mtoro M, Maboko MAH, Manya S (2009) Geochemistry and geochronology of the bimodal volcanic rocks of the Suguti area in the southern part of the Musoma-Mara Greenstone Belt, Northern Tanzania. Precambrian Res 174:241–257

Nash BP, Perkins ME, Christensen JN, Lee D-C, Halliday AN (2006) The Yellowstone hotspot in space and time: Nd and Hf isotopes in silicic magmas. Earth Planet Sci Lett 247(1–2):143–156

Notsu K, Fujitani T, Ui T, Matsuda J, Ercan T (1995) Geochemical features of collision-related volcanic rocks in central and eastern Anatolia, Turkey. J Volcanol Geotherm Res 64:171–192

Okay AI, Tüysüz O (1999) Tethyan sutures of northern Turkey. In: Durand B, Jovilet L, Horva THF, Seranne M (eds) The Mediterranean basin: tertiary extension within the Alpine orogen. Geol Soc London Spec Publ 156:475–515

Paces JB, Miller JD (1993) Precise U–Pb ages of Duluth Complex and related mafic intrusions, northeastern Minnesota: geochronological insights to physical, petrogenetic, paleomagnetic, and tectonomagmatic processes associated with the 1.1 Ga Midcontinent Rift System. J Geophys Res: Solid Earth (1978–2012), 98(B8):13997–14013

Parlak O, Höck V, Delaloye M (2002) The supra-subduction zone Pozanti-Karsanti ophiolite, southern Turkey: evidence for high-pressure crystal fractionation of ultramafic cumulates. Lithos 65:205–224

Pasquare G, Poli S, Vezzoli L, Zanchi A (1988) Continental arc volcanism and tectonic setting in Central Anatolia, Turkey. Tectonophysics 146:217–230

Pearce JA (1982) Trace element characteristics of lavas from destructive plate boundaries. In: Thorpe RS (ed) Andesites: Orogenic andesites and plate tectonics. Wiley, Chichester, pp 525–548

Pearce JA, Bender JF, de Long SE, Kidd WSF, Low PJ, Güner Y, Şaroğlu F, Yılmaz T, Moorbath S, Mitchell JG (1990) Genesis of collision volcanism in eastern Anatolia, Turkey. J Volcanol Getherm Res 44:189–229

Peccerillo A, Taylor SR (1976) Geochemistry of Eocene calc-alkaline volcanic rocks from the Kastamonu area, Northern Turkey. Contrib Mineral Petrol 58:63–81

Peccerillo A, Barberio MR, Yirgu G, Ayalew D, Barbieri M, Wu TW (2003) Relationship between mafic and peralkaline felsic magmatism in continental rift settings: a petrological, geochemical and isotopic study of the Gedemsa Volcano, Central Ethiopian Rift. J Petrol 44:2003–2032

Pe-Piper G, Moulton B (2008) Magma evolution in the Pliocene-Pleistocene succession of Kos, South Aegean arc (Greece). Lithos 106(1–2):110–124

Perini G, Francalanci L, Davidson JP, Conticelli S (2004) The petrogenesis of Vico Volcano, Central Italy: an example of low scale mantle heterogeneity. J Petrol 45:139–182

Piromallo C, Morelli A (2003) P wave tomography of the mantle under the Alpine-Mediterranean area. J Geophys Res 108(B2):2065. doi:10.1029/2002JB001757

Reid MR, Coath CD, Harrison TM, McKeegan KD (1997) Prolonged residence times for the youngest rhyolites associated with Long Valley Caldera; 230Th- 238U ion microprobe dating of young zircons. Earth Planet Sci Lett 150(1–2):27–39

Reilinger RE, McClusky SC, Oral MB (1997) Global positioning system measurements of present day crustal movements in the Arabian-african-Eurasian plate collision zone. J Geophys Res 102:9983–9999. doi:10.1029/96JB03736

Robertson AHF, Grasso M (1995) Overview of the late Triassic-recent tectonic and palaeo-environmental development of the Mediterranean region. Terra Nova 7:114–127

Rooney T, Hart W, Hall C, Ayalew D, Ghiorso M, Hidalgo P, Yirgu G (2012) Peralkaline magma evolution and the tephra record in the Ethiopian Rift. Contrib Mineral Petrol 164(3):407–426

Rudnick RL, Gao S (2004) Composition of the continental crust. In: Holland HD, Turekian KK (eds) Treatise on geochemistry, vol 3. Elsevier, Amsterdam, pp 1–64

Sage RP, Lightfoot PC, Doherty W (1996) Bimodal cyclical Archean basalts and rhyolites from the Michipicoten (Wawa) greenstone belt, Ontario: geochemical evidence for magma contributions from the asthenospheric mantle and ancient continental lithosphere near the southern margin of the Superior Province. Precambrian Res 76:119–153

Sañudo-Wilhelmy SA, Flegal AR (1994) Temporal variations in lead concentrations and isotopic composition in the Southern California Bight. Geochim Cosmochim Acta 58(15):3315–3320

Schmitt AK, Grove M, Harrison TM, Lovera O, Hulen J, Walters M (2003) The Geysers-Cobb Mountain Magma System, California (Part 1): U–Pb zircon ages of volcanic rocks, conditions of zircon crystallization and magma residence times. Geochim Cosmochim Acta 67(18):3423–3442

Schmitt AK, Danisîk M, Evans N, Siebel W, Kiemele E, Aydin F, Harvey JC (2011) Acıgöl rhyolite field, Central Anatolia (part 1): high-resolution dating of eruption episodes and zircon growth rates. Contrib Mineral Petrol 162:1215–1231

Şengör AMC, Kidd WSF (1979) Post-collisional tectonics of the Turkish-Iranian plateau and a comprasion with Tibet. Tectonophysics 55:361–376

Şengör AMC, Yılmaz Y (1981) Tethyan evolution of Turkey.A plate tectonic approach. Tectonophysics 75:181–241

Şengör AMC, Görür N, Şaroğlu F (1985) Strike slip faulting and related basin formation in zones of tectonic escape: Turkey as

a case study. In Biddle TR, Christie-Blick N (eds) Strike-slip deformation, basin formation and sedimentation. Soc Econ Paleontol Min Spec Publ 37:227–264

Siebel W, Schmitt AK, Kiemele E, Danišík M, Aydin F (2011) Acıgöl rhyolite field, central Anatolia (Part II): geochemical and isotopic (Sr-Nd-Pb, $\delta^{18}O$) constraints on volcanism involving two high-silica rhyolite suites. Contrib Mineral Petrol 162:1233–1247

Simon JI, Renne PR, Mundil R (2008) Implications of pre-eruptive magmatic histories of zircons for U–Pb geochronology of silicic extrusions. Earth Planet Sci Letters 266(1–2):182–194

Smith EI, Sanchez A, Walker JD, Wang K (1999) Geochemistry of mafic magmas in the Hurricane volcanic field, Utah: implications for small- and large-scale chemical variability of the lithospheric mantle. J Geol 107:433–448

Steiger RH, Jäger E (1977) Subcommission on geochronology-convention on use of decay constants in geochronology and cosmochronology. Earth Planet Sci Lett 36(3):359–362

Sun SS, McDonough WE (1989) Chemical and isotopic systematics of oceanic basalts: implications for mantle composition an processes. In: Saunders AD, Norry MJ (eds) Magmatism in the ocean basins. Geol Soc London Spec Publ, pp 313–345

Tatar O, Gürsoy H, Piper DD (2002) Differential Neotectonic rotations in Anatolia and the Tauride Arc: paleomagnetic investigation of the Erenlerdağ Volcanic Complex and Isparta volcanic district, South-central Turkey. J Geol Soc Lond 159:281–294. doi:10.1144/0016-764901-035

Temel A, Gündoğdu MN, Gourgaud A, Le Pennec J-L (1998) Ignimbrites of Cappadocia (Central Anatolia, Turkey): petrology and geochemistry. J Volcanol Geotherm Res 85:447–471

Thompson RN (1972) Evidence for a chemical discontinuity near the basalt-andesite transition in many anorogenic volcanic suites. Nature 236:106–110

Toprak V (1998) Vent distribution and its relation to regional tectonics, Cappadocian Volcanics, Turkey. J Volcanol Geotherm Res 85:55–67

Toprak V, Göncüoğlu MC (1993) Tectonic control on the evolution of the Neogene-Quaternary Central Anatolian Volcanic Province, Turkey. Geol J 28:357–369

Trail D, Mojzsis SJ, Harrison TM, Schmitt AK, Watson EB, Young ED (2007) Constraints on Hadean zircon protoliths from oxygen isotopes, Ti-thermometry, and rare earth elements. Geochem Geophys Geosyst 8:Q06014. doi:10.1029/2006GC001449

Türkecan A, Akçay AE, Satır M, Dönmez M, Ercan T (2003) Melendiz dağları (Niğde) volkanizması. In: 56th geological congress of Turkey, extended abstracts, Ankara, pp 16–17

Turner S, Sandiford M, Foden J (1992) Some geodynamic and compositional constraints on "postorogenic" magmatism. Geology 20:931–934

Van Wagoner NA, Leybourne MI, Dadd KA, Baldwin DK, McNeil W (2002) Late Silurian bimodal volcanism of southwestern New Brunswick, Canada: products of continental extension. Geol Soc Am Bull 114:400–418

Vazquez JA, Reid MR (2004) Probing the accumulation history of the voluminous Toba magma. Science 305:991–994

Wang KL, Chung SL, O'Reilly SY, Sun SS, Shinjo R, Chen CH (2004) Geochemical constraints for the genesis of post-collisional magmatism and geodynamic evolution of the Northern Taiwan Region. J Petrol 45:975–1011

Whalen JB, Currie KL, Chappell BW (1987) A-type granites: geochemical characteristics, discrimination and petrogenesis. Contrib Mineral Petrol 95:407–419

Whitney DL, Dilek Y (1997) Core complex development in central Anatolia. Geology 25:1023–1026

Whitney DL, Dilek Y (1998) Metamorphism during crustal thickening and extension in central Anatolia: The Niğde metamorphic core complex. J Petrol 39:1385–1403

Wilson M (1989) Igneous petrogenesis. Unwin Hyman, London

Wotzlaw J-F, Schaltegger U, Frick DA, Dungan MA, Gerdes A, Gunther D (2013) Tracking the evolution of large-volume silicic magma reservoirs from assembly to supereruption. Geology 41:867–870

Yang JH, Chung SI, Zhai MG, Zhou XH (2004) Geochemical and Sr–Nd–Pb isotopic compositions of mafic dykes from the Jiaodong peninsula, China: evidence for vein-plus-peridotite melting in the lithospheric mantle. Lithos 73:145–160

Yılmaz Y (1993) New evidence and model on the evolution of the Southeast Anatolian orogeny. Geol Soc Am Bull 105:251–271

Zhang XH, Zhang H, Tang Y, Wilde SA, Hu Z (2008) Geochemistry of Permian bimodal volcanic rocks from central Inner Mongolia, North China: implications for tectonic setting and Phanerozoic continental growth in Central Asian Orogenic Belt. Chem Geol 249:262–281

Zindler A, Hart S (1986) Chemical geodynamics. Annu Rev Earth Planet Sci 14:493–571